SPECIAL REPORT 92-13

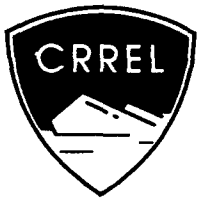

Unconventional Energy Sources for Ice Control at Lock and Dam Installations

Tatsuaki Nakato, Robert Ettema and Keiichi Toda

June 1992

For conversion of SI metric units to U.S./British customary units of measurement consult ASTM Standard E380, Metric Practice Guide, *published by the American Society for Testing and Materials, 1916 Race St., Philadelphia, Pa. 19103.*

This report is printed on paper that contains a minimum of 50% recycled material.

Special Report 92-13

U.S. Army Corps of Engineers
Cold Regions Research & Engineering Laboratory

Unconventional Energy Sources for Ice Control at Lock and Dam Installations

Tatsuaki Nakato, Robert Ettema and Keiichi Toda

June 1992

Prepared for
OFFICE OF THE CHIEF OF ENGINEERS

PREFACE

This report was prepared by Tatsuaki Nakato, Research Scientist; Robert Ettema, Research Engineer; and Keiichi Toda, Research Assistant, Iowa Institute of Hydraulic Research, The University of Iowa, Iowa City, Iowa. Funding was provided by the Office of the Chief of Engineers, Directorate of Civil Works, under the River Ice Management program, Contract No. DACW89-86-K-001.

The investigation was conducted for and sponsored by the U.S. Army Corps of Engineers (COE), Cold Regions Research and Engineering Laboratory (CRREL), Hanover, New Hampshire, under the River Ice Management (RIM) program. The authors express their thanks to Kevin Carey and Dr. George Ashton of CRREL for their unfailing cooperation throughout the study and for critically reviewing the final report. Thanks are due to the COE personnel in the Rock Island District, St. Paul District and Pittsburgh District, who assisted the authors in arranging field trips to various locks and dams. Many lockmasters provided the authors with valuable information on ice control, and many more COE representatives from various districts provided the authors with useful comments during the RIM review meetings. Finally, the authors acknowledge Michael Kundert of the Iowa Institute of Hydraulic Research, The University of Iowa, for his excellent drafting.

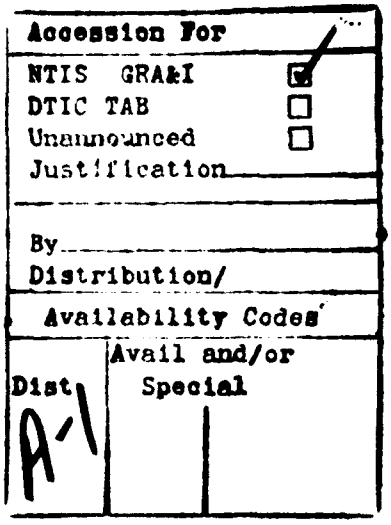

CONTENTS

ILLUSTRATIONS

TABLES

Unconventional Energy Sources for Ice Control at Lock and Dam Installations

TATSUAKI NAKATO, ROBERT ETTEMA AND KEIICHI TODA

INTRODUCTION

A major concern for operating a navigation lock and dam during frigid weather is ice formation along lock walls, at lock miter gates and at dam gates. Ice collars create numerous operational problems, including reducing the effective lock width, creating difficulty in operating miter gates, interfering with vessel passage and making it necessary to reduce tow width. Gates made inoperable by being frozen to ice sheets, or by becoming encrusted in ice, pose potentially adverse consequences for flow regulation. It is therefore extremely important that appropriate methods be found for controlling ice growth at lock and dam installations.

Two general methods can be adopted for controlling ice growth: mechanical and thermal. Mechanical methods, which involve removing ice that has already formed, are part of routine operations generally followed at locks and dams. A variety of devices are used to remove ice, including backhoe scrapers, chainsaw cutters, pike poles, high-pressure water jets and steam jets. These methods, however, can be arduous and occasionally hazardous. Thermal methods entail two alternatives: a) applying sufficient waste heat available from, for example, a power plant to keep the temperature of water in the lock chamber above its freezing temperature; or b) keeping lock walls, gates and pier walls adequately warm, in the vicinity where ice would form, such that ice growth is inhibited.

Conventional energy sources, primarily electricity from power-generation utilities or hydrocarbon fuels, have proven to be comparatively expensive when used for ice control at lock and dam installations. Therefore, unconventional energy sources, such as solar energy, wind energy and sensible heat from groundwater, appear attractive. This investigation assesses the feasibilities of various unconventional energy sources for ice control. It includes a review, through several site visits, of ice-control practices generally used at lock and dam installations. Also discussed are the heating requirements for ice control at locks and the characteristics of heat transfer through concrete lock walls or pier walls.

ICE-GROWTH PROBLEMS AT NAVIGATION LOCKS AND DAMS

The two ice-growth processes of concern are ice-collar formation along lock walls and lock miter gates, and ice growth against dam gates. Under most circumstances, ice-collar growth is a form of border (or shorefast) ice growth, forming at the water-surface elevation predominantly maintained in a lock (Fig. 1). This may be at either the upstream or the downstream pool elevation, depending on individual lock operation practice. Or, as it is fairly common to allow some continuous throughflow of water to inhibit ice-cover formation over the entire lock chamber, an ice collar may form at an elevation between these pool elevations.

Relatively quiescent water adjoining the walls of a lock experiences less vertical mixing of flow and more rapid cooling of the flow surface than the water toward the center of the lock. Consequently, as is the case with many water bodies exposed to frigid air, ice growth commences at fixed boundaries and then thickens and progresses toward the center of the lock. Raising and lowering the water level within the lock, together with accumulation of snow, frazil and ice debris and abrasion during barge impact, cause ice collars to become somewhat rounded in cross section. Although the dimensions of ice collars vary with growth conditions, typical maximum dimensions reported by Corps of Engineers (COE) personnel are up to 1 m in height and 1 m in depth (Fig. 2). Under some circumstances, it may be possible for ice growth to extend down much of the lock lift height. Conceivably, this might occur if a series of collars are allowed to form because the water surface is held for significant periods at several elevations. Alternatively,

Figure 1. Ice-collar growth along lock walls of Starved Rock Lock and Dam, Illinois River, January 1982.

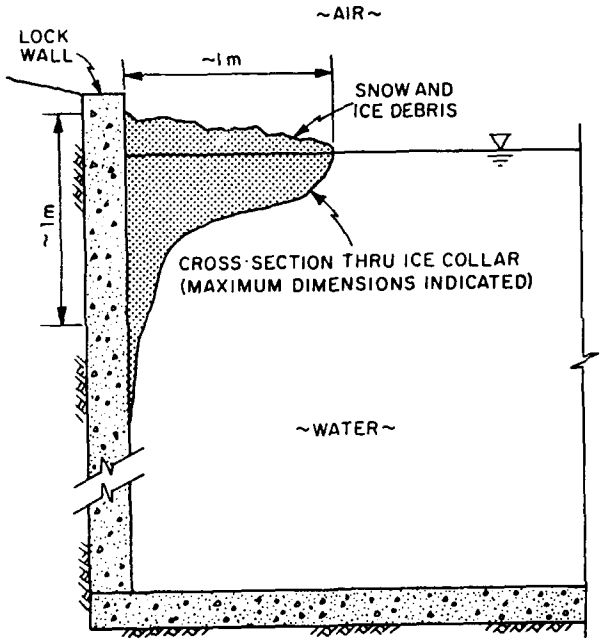

Figure 2. Typical geometry and maximum dimensions of ice collars.

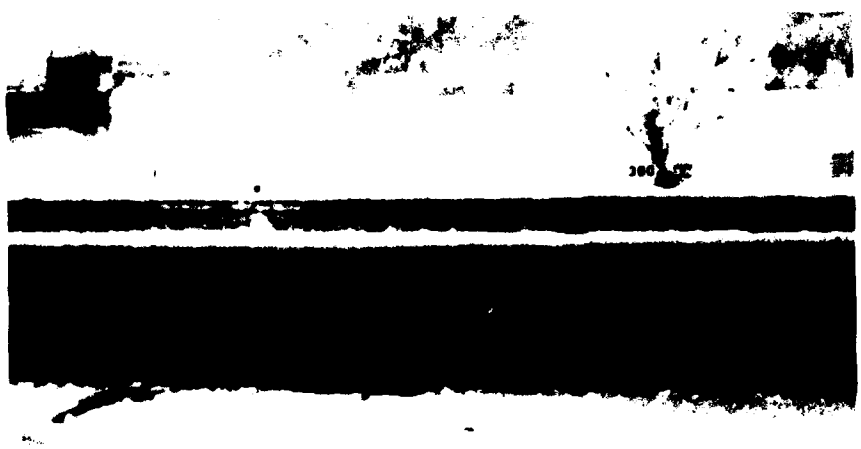

Figure 3. Icing over a lock wall below an ice collar at Starved Rock Lock and Dam, Illinois River, 4 February 1978.

Figure 4. Ice sheet immediately upstream from L&D No. 5 on the Mississippi River, 23 January 1986.

Figure 5. Tainter gate with splash and spray icing at L&D No. 5 on the Mississippi River, 26 January 1986.

repeated wetting of lock walls may cause ice to accrete as an icing (Fig. 3). Such icing of lock walls is usually less problematical than ice-collar growth.

Ice-growth problems on dam gates originate from several causes:

- Upstream gate faces may become frozen and stuck to adjoining river ice covers (Fig. 4);
- Ice growth due to water splash and spray, on the rear of gates as well as areas surrounding tainter-gate trunnions and roller-gate ring-gear and rack devices, may render them inoperable (Fig. 5).
- Gates may become unbalanced by uneven ice growth such that they are difficult to operate; and
- Gate side seals are prone to ice accretion because of water seepage as well as water splash and spray.

Sometimes, due to the effects of water-level fluctuations, a crack separates the ice cover from ice formed as a collar along the gate face and gate piers (Fig. 5).

Ice problems at locks and dams and in navigable waterways are discussed by Zufelt and Calkins (1985). They provided a summary of problem severity for the Allegheny, Illinois, Mississippi and Ohio rivers.

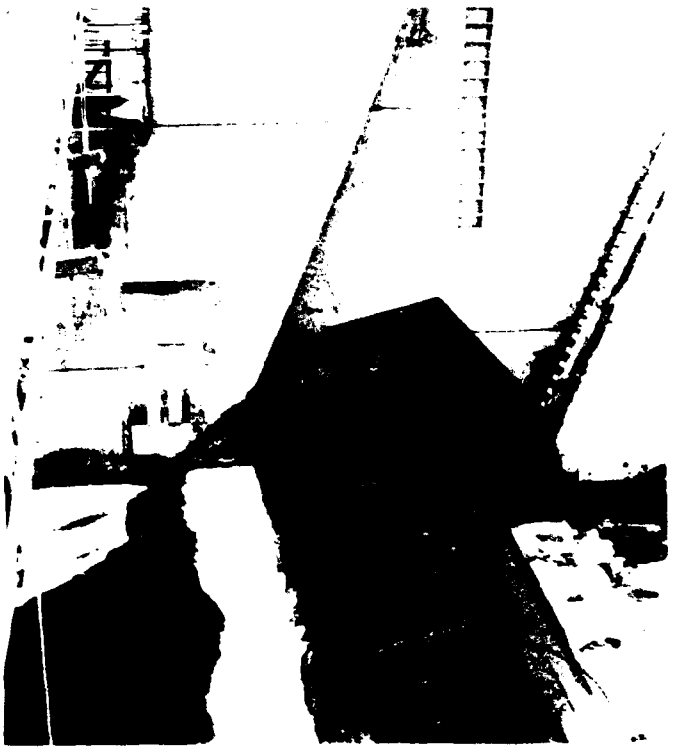

Figure 6. Side-seal heaters embedded in a roller-gate pier wall at L&D No. 6 on the Mississippi River, 26 January 1986.

Figure 7. Quartz heaters suspended over a roller-gate rack at L&D No. 6 on the Mississippi River, 26 January 1986.

FIELD PRACTICES FOR ICE CONTROL

To review current ice-control practices, we visited several lock and dam (L&D) installations during January and March 1986. Lockmasters were interviewed regarding ice-control problems and practices. Because of the limited number of site visits, the following comments, which are based on the daily experience of the lockmasters interviewed, are not necessarily conclusive.

We visited two locks and dams on the Mississippi River (L&D No. 5 at Minnesota City, Minnesota, and L&D No. 6 at Trempealeau, Wisconsin). Most lock facilities on the Mississippi River are generally closed when thick ice forms in the river. However, dam gate structures must be operational, even during severe winter months, to control river stages. Therefore, much emphasis seemed to be focused on how to keep large roller gates ice-free. At L&D No. 5 a large carriage-mounted steamer is used in conjunction with steam lances to de-ice dam gates. Both installations use electric side-seal heaters embedded in the roller-gate pier walls. Three side-seal heating elements (2.3 kW per element) that operate together are placed in each pier wall pocket (Fig. 6). The lockmaster of L&D No. 6 said that de-icing with side-seal heaters can be accomplished within about 45 minutes of their application. Quartz heaters (2.5-kW units) are also used extensively to melt ice that forms on gate racks. Figure 7 shows two quartz heaters being suspended over a roller-gate rack.

The power requirements for controlling ice growth on dam gates at these L&Ds can be estimated on the basis of these heater capacities. Consider, for example, L&D No. 5, which is equipped with six 6.1-m-high, 18.3-m-long roller gates. If two quartz heaters ($2 \times 2.5 = 5$ kW) and three side-seal heaters ($3 \times 2.3 = 6.9$ kW) are used for each pier wall, a total of 142.8 kW would be needed. Because three or four roller gates are generally sufficient to regulate low winter river flows, only half of this power would be required to keep three roller gates ice-free.

At Marseilles L&D (Marseilles, Illinois) on the Illinois River, electrical heating cables were installed on the top of the miter gates to keep the gates ice-free. Insulation pads were placed over the heating area. Quartz heaters similar to those used on the Mississippi River installations were tried around miter-gate hinges. However, they were found to be ineffective. Instead, high-pressure water jets were used to wash solid ice off gate quoin areas. The reason quartz heaters failed to work here is that Marseilles Lock is operational during most of the winter. Therefore, areas surrounding gate hinges are subject to frequent changes in water-surface elevation, which would produce thicker ice than in the roller-gate case, where ice forms more slowly from a combination of spray and seepage water. Large-scale transverse bubbler systems were also used to deflect ice away from miter-gate recesses. The bubbler systems must be kept running continuously to avoid pipe-freezing problems. Properly designed bubbler systems generally do not require continuous operation.

Three L&D facilities were visited on the Ohio River. Emsworth L&D, located at Emsworth, Pennsylvania, uses bubbler systems extensively in miter-gate recesses as well as near the approach and exit sills of the lock chamber. A hydropower generator rated at 300 kW was newly in service to provide the power for general operation and for ice control. The utility bill without turbine output during the winter was about four times larger than that with the operating turbine. Dashields L&D at Glenwillard, Pennsylvania, has an ungated fixed-crest dam, so it does not experience gate-related ice problems. A large air-bubbler system with a 0.17-m^3/s compressor is used to flush ice away from miter-gate recesses. Kerosene-burner-type heaters, with capacities of 44 kWh per unit, are lowered along lock walls to melt ice collars formed there. Montgomery L&D at Industry, Pennsylvania, is similar to Emsworth L&D. The normal lift at this site is about 5.5 m, which promises a great potential for hydropower development.

L&D No. 7 at West Kittanning, Pennsylvania, and L&D No. 8 at Templeton, Pennsylvania, on the Allegheny River were visited. Both L&Ds have fixed-crest dams, and there is no navigation during severe, icy winter days. Neither heating facilities nor bubblers were used there. Only manpower with chipping hammers and pike poles was utilized to remove solid ice formed on the lock walls and miter gates.

Ice-control measures seem to depend largely on each lockmaster's preference. For example, the lockmaster at L&D No. 6 on the Mississippi River routinely shakes all roller gates to prevent formation of thick solid ice on gate structures. The frequency of this loosening operation generally depends on the weather.

It was the consensus of the lockmasters interviewed that, during typical winters, they are able to control ice problems. This opinion, again, does not necessarily represent the general opinion concerning difficulties in controlling ice at other lock and dam installations. They all agreed, however, that recently installed heaters and air bubblers had significantly alleviated many safety concerns. Without them, manpower was the only means of coping with ice problems under extremely treacherous conditions. Besides safety, operational efficiency had been greatly improved with heating systems.

POWER REQUIREMENTS

In this section, power requirements for lock wall ice control are estimated, and heat-transfer characteristics for a heat source embedded in a concrete lock wall are discussed.

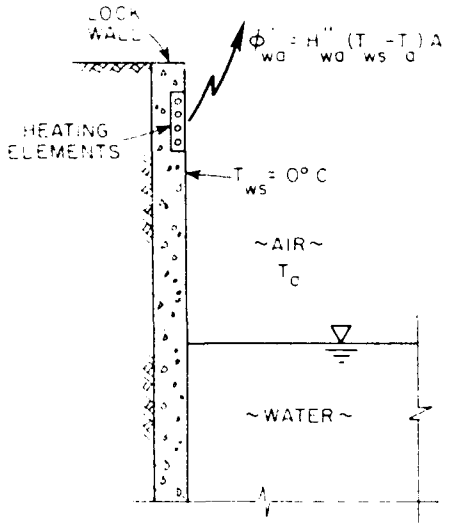

Figure 8. Heat transfer at a lock wall.

Heat loss from a boundary exposed to frigid air is generally estimated in terms of a linear combination of an overall heat-transfer coefficient and the temperature difference between the boundary and air. For example, a rate of heat transfer associated with a band of lock wall o''_{wa}, as shown in Figure 8, can be expressed as

$$o''_{wa} = H''_{wa}(T_{ws} - T_a)\,A \qquad (1)$$

where H''_{wa} = heat-loss coefficient
T_{ws} = wall-surface temperature (°C)
T_a = air temperature (°C)
A = surface area.

A value of 20 W/m^2·°C is commonly used for the heat-loss coefficient.* To justify the use of this value, several references were surveyed. According to Dickinson and Cheremisinoff (1980), heat-loss coefficients may be as high as 30–60 W/m^2·°C if an unglazed solar-energy absorber plate is used as a solar-energy collector. They also reported that this value can be reduced to 5–10 W/m^2·°C by the use of one glazed cover. Therefore, the use of 20 W/m^2·°C for the heat-loss coefficient in the present case appears to be justified.

* Unpublished notes, G.D. Ashton, 1985.

In accordance with eq 1 and with T_{ws} = 0°C, the power loss per unit area of lock wall surface, o''_{wa}/A, is 100 W/m^2 when T_a = –5°C, 200 W/m^2 when T_a = –10°C, and 500 W/m^2 when T_a = –25°C.

Two references reporting experiences with heating of lock walls to inhibit ice growth corroborate these estimates of power losses. Thomas (1976) and Frankenstein and Wortley (1984) described a system of electric heating cables spaced 0.15 m apart and embedded in 0.076-m slots cut in a lock wall at St. Lambert Lock on the St. Lawrence Seaway. A power intensity of approximately 160 W/m^2 proved effective in preventing an ice collar from forming when the air temperature was –5.6°C. Balanin et al. (1986) reported the successful use of metal heating strips buried in concrete lock walls. They reported that 500–600 W/m^2 applied for three hours with an air temperature of –20°C was usually sufficient to weaken ice growth 0.15–0.20 m thick such that, under its own weight, it fell off lock walls. To reduce the power requirements for de-icing, Balanin et al. (1986) suggested that the heating be performed intermittently at a sequence of zones along the lock walls.

For ice control on lock walls, it is essential to supply enough power to overcome the power loss from the lock wall boundary. Our study, therefore, set out to determine the heat-transfer characteristics of heating sources placed in concrete lock walls. The resulting mathematical analysis is summarized in Appendix A. Several configurations of heat sources were considered: a continuous planar heat source embedded in the lock wall; a line heat source embedded in the lock wall; a rectangular boundary containing two heat sources; and a triangular pocket containing two line heat sources. The latter two configurations simulate the use of two heating rods inserted in slots to inhibit ice formation on roller-gate seals. Each analysis included temporal distributions of temperature within the concrete boundary, the temporal rate of heat transfer at the concrete–air boundary, and the total thermal energy expended after prescribed times of application. The results, included in Appendix A, are presented in a normalized format so as to be useful for general estimates of heating requirements for concrete walls.

A simple, one-dimensional, heat-diffusion analysis for a planar heat source embedded in a concrete wall (Fig. A1) can provide useful engineering information on heating requirements for lock walls. Consider, for example, the case when the lock wall surface is at 0°C and a heat insulator is placed at $x = b$ (Fig. A1). When a planar heat source is placed at $x = x'$, temporal variations of heat transfer at the lock wall boundary ($x = 0$) H_1 can be computed for various values of power intensity $Q/(BH)$, in which Q is the total power applied (W), B is

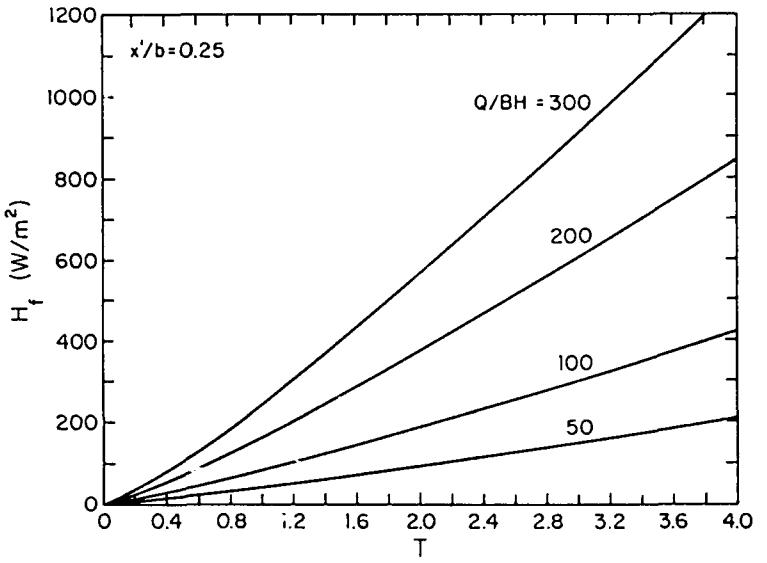

Figure 9. Temporal variations of H_f *for different* Q/BH *values* (x′/b = *0.25*).

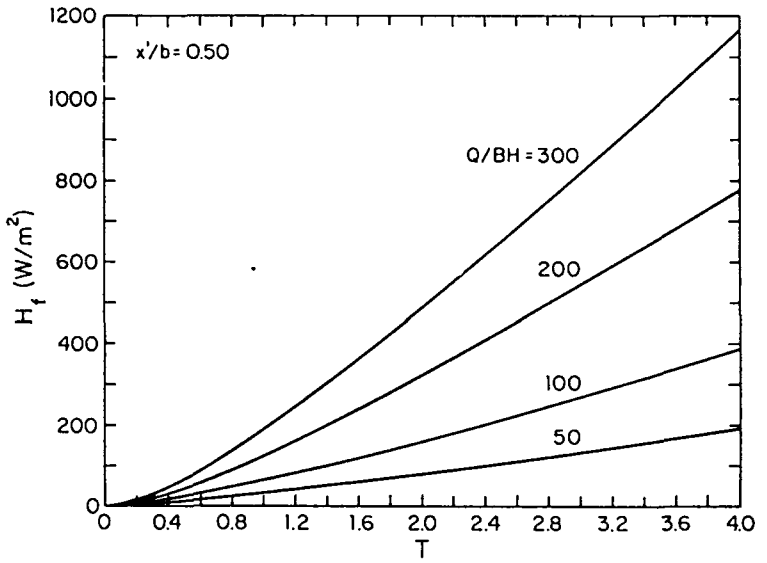

Figure 10. Temporal variations of H_f *for different* Q/BH *values* (x′/b = *0.50*).

the lock wall length (m) and H is the lock wall height (m). Figure 9 shows the relationship between T and H_f for a range of $Q/(BH)$ varying from 50 to 300 W/m^2 for $x'/b = 0.25$, in which T is normalized time $[kt/(b^2)]$, k is the heat diffusivity of concrete (4.2×10^{-7} m^2/s) and t is time (s). Similar relationships are depicted in Figure 10 for $x'/b = 0.50$. As can be seen from these figures, the same H_f value for a given $Q/(BH)$ value can be reached in a shorter time when the heat source is located closer to the lock wall surface.

To demonstrate the practical use of these figures, the effect of the power intensity $Q/(BH)$ on the time required for supplying 200 W/m^2 of heat at the lock wall surface was evaluated for $b = 0.10$ m, the result of which is shown in Table 1. The relative location of the heating element x'/b was also varied for this case. In accordance with eq 1, $H_f = 200$ W/m^2 corresponds to a case in which the air temperature is –10°C, assuming that the heat-transfer coefficient is 20 W/m^2·°C and $T_{ws} = 0$°C. Table 1 shows that, for example, it takes about 5.6 hours if the heater with an intensity of 300 W/m^2 is located 0.025 m from the lock wall surface, and about 7.9 hours if the intensity is 200 W/m^2. If the heating element is placed 0.05 m from the lock wall surface under the same conditions, the time to satisfy $H_f = 200$ W/m^2 is about 6.8 hours and 9.2 hours for $Q/(BH) = 300$ and 200 W/m^2, respectively. By using Figures 9 and 10, similar estimates could be easily obtained for different values of b.

The effect of the relative location of the heating element on the rate of heat transfer at the lock wall boundary was also analyzed. Figure 11 demonstrates the variation of H_f in time for different values of x'/b for $Q/(BH) = 100$ W/m^2. As expected, this figure shows that a larger heat transfer rate is obtainable with a smaller value of x'/b. Table 2 illustrates the relative importance of x'/b on H_f for $b = 0.10$ m. After 6.61 hours of heat

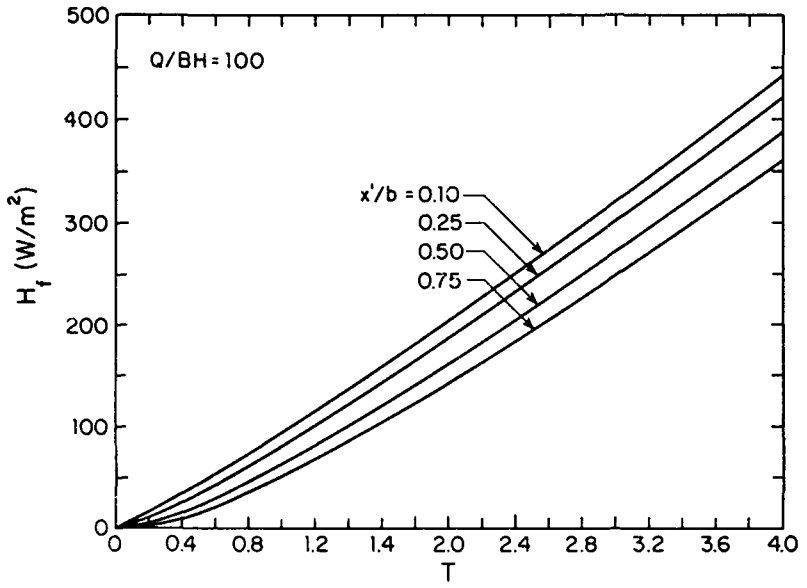

Figure 11. Temporal variations of H_f *for different* x'/b *values* (Q/BH = *100* W/m^2).

Table 1. Effect of heat-source intensity and location of heating element on the time required for supplying a rate of heat transfer of 200 W/m² at the lock wall surface (one-dimensional model).

x'/b = 0.25			x'/b = 0.50		
Q/(BH) (W/m^2)	T	t (hours)	Q/(BH) (W/m^2)	T	t (hours)
50	3.82	25.26	50	4.09	27.05
100	2.11	13.96	100	2.35	15.54
200	1.19	7.87	200	1.39	9.19
300	0.85	5.62	300	1.03	6.81

Notes:
Heat-transfer rate: H_f = 200 W/m².
Plane power source: Q (W).
Lock wall surface area: BH (m²).
Location of heating element: $x = x'$.
Concrete lock wall thickness: b = 0.10 m.
Heat diffusivity of concrete: $k = 4.2 \times 10^{-7}$ m²/s.
$T = kt/(b^2)$.

Table 2. Effect of heating-element location on the rate of heat transfer at the lock wall surface (one-dimensional model).

	H_f (W/m^2)			
x'/b	t = 6.61 hr	t = 13.23 hr	t = 19.84 hr	t = 26.46 hr
0.10	94.08	204.18	321.59	443.51
0.25	81.37	187.37	302.11	412.92
0.50	63.72	162.70	272.85	389.11
0.75	51.28	143.59	249.08	361.68

Notes:
Heat-source strength: $Q/(BH)$ = 100 W/m².
Lock wall surface area: BH (m²).
Location of heating element: $x = x'$.
Concrete lock wall thickness: b = 0.10 m.
Heat diffusivity of concrete: $k = 4.2 \times 10^{-7}$ m²/s.

application at a power intensity of 100 W/m², the rate of heat transfer at the lock wall surface would be about 94, 81, 64 and 51 W/m² for $x'/b = 0.10, 0.25, 0.50$ and 0.75, respectively. After about 20 hours the rate of heat transfer would be about 322, 302, 273 and 249 W/m² for $x'/b = 0.10, 0.25, 0.50$ and 0.75, respectively.

This analysis is based on a one-dimensional model that utilizes an idealized boundary condition under which the temperature of the lock wall surface is assumed to be 0°C due to ice attached to the lock wall. Also, it involves the assumption that a heat insulator is placed at $x = b$ such that the temperature gradient there is zero. The resulting power evaluations, therefore, are intended for approximately assessing the required power and time to maintain a lock wall ice-free.

FEASIBILITY OF UNCONVENTIONAL ENERGY SOURCES

In the preceding section, power requirements for ice control in navigation locks were assessed. In this section, groundwater energy, solar energy, wind energy and microhydropower energy are evaluated as potential energy sources for meeting these power requirements.

Groundwater energy

Groundwater energy appears to be an attractive energy source for use in ice control at lock and dam installations. It is readily available in the vicinity of many rivers, and year-round its temperature generally remains at the average annual air temperature of the locality (Fig. 12). However, its attractiveness is somewhat diminished by practical problems associated with its implementation. Additionally, the farther north (in the

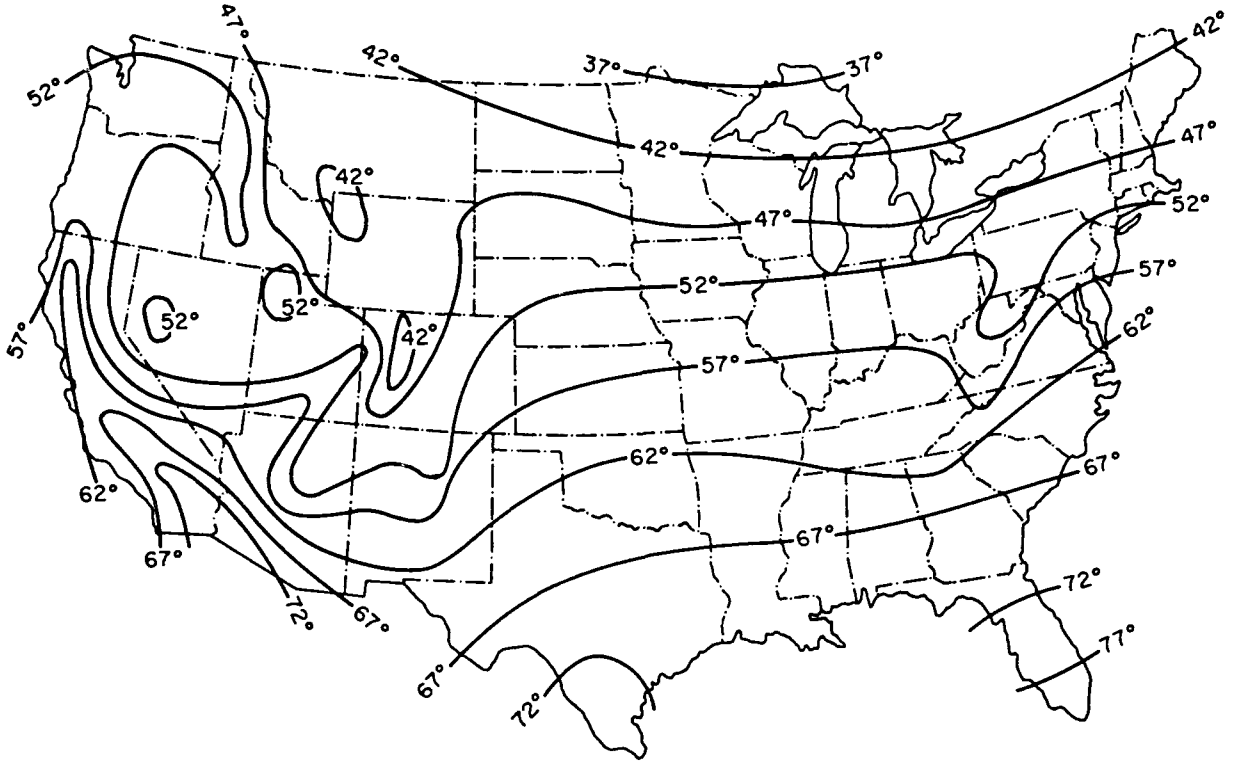

Figure 12. Typical groundwater temperatures in the United States. (After Johnson 1966.)

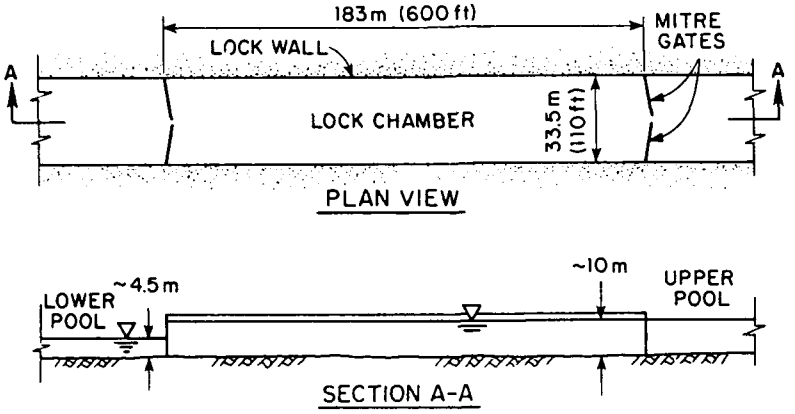

Figure 13. Typical dimensions of a lock (Starved Rock Lock and Dam, Illinois River).

northern hemisphere) one goes, the less attractive it becomes because the groundwater temperature decreases.

In this section, the power to heat lock water, the power to heat water near lock walls, and the heat-transfer characteristics of groundwater flow through pipes placed in lock walls are analyzed separately.

Power to heat water in locks

Ashton* examined the feasibility of pumping groundwater into a lock chamber with the objective of maintaining the water temperature above freezing temperature. His analysis is repeated and extended here.

Of interest in the analysis are the discharge of groundwater required and the power likely needed in delivering it to a representative lock. Ashton assumed that

- A sufficient quantity of groundwater is available;
- A typical groundwater temperature T_g is 5.6°C, based on the mean annual air temperature;
- The river water is at the freezing temperature, i.e. $T_w = 0$°C;
- An appropriate heat-transfer coefficient from water to air is 20 W/m^2·°C;
- Standard lock dimensions are 183 × 33.5 m in plan and 10 m in depth if the lock chamber is held at the

* Personal communication, CRREL, 1985.

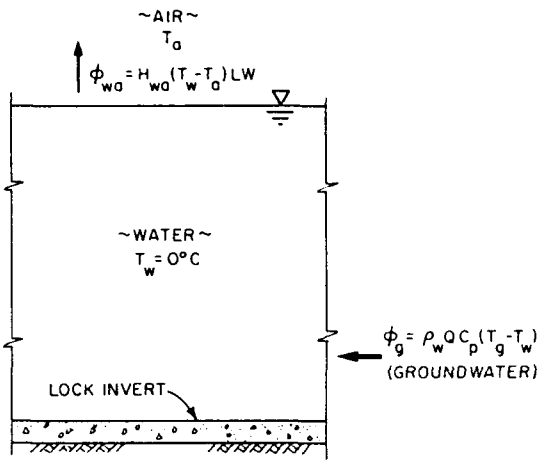

Figure 14. Heat transfer at a lock chamber.

upper pool level or 4.5 m in depth if held at the lower pool level (Fig. 13); and

- No river water flows through closed locks.

This analysis also considers discharge requirements for a groundwater temperature of 12.2°C, as a reasonable maximum value of groundwater temperature (Fig. 12), especially for locks located on the central portions of the Ohio and Mississippi rivers.

The rate of heat loss from the water surface in the lock chamber, as shown in Figure 14, can be determined from

$$\phi_{wa} = H_{wa}(T_w - T_a)LW \qquad (2)$$

in which L is the inside length of the lock and W is the inside width of the lock. The rate of heat added to the lock by introducing groundwater is

$$\phi_g = \rho_w Q c_p (T_g - T_w) \qquad (3)$$

where Q = discharge of pumped groundwater
ρ_w = water density
c_p = specific heat of water (4.2 kJ/kg·°C).

Equating eq 2 and 3 yields an expression for values of Q in order to maintain T_w = 0°C in the lock under different values of air temperature:

$$Q = -(H_{wa}T_a LW)/(\rho_w c_p T_g). \qquad (4)$$

Table 3 lists the requisite values of Q associated with T_a = –5 to –25°C and T_g = 5.6 and 12.2°C. As expected, less warm groundwater is needed for the larger value of T_g.

A concern to be borne in mind, however, is that river water at 5.6°C is denser than at 0°C; the peak density occurs at 4°C. Consequently groundwater would sink to the bottom of the lock such that lock water would become thermally stratified, and ice may form over its surface. To prevent this the lock either would have to be filled completely with groundwater or the lock water would have to be mixed mechanically by means of air bubblers or water jets.

If no mechanical mixing is provided, groundwater would cool from 5.6°C to about 4°C before settling to the lower portion of the lock. Under this condition, values of Q in Table 3 should be multiplied by 3.5 [= 5.6/(5.6 – 4.0)] to ensure that T_w at the water surface does not drop below 0°C. If, for example, T_a = –15°C, then Q = 0.275 m^3/s. At this discharge, however, a 183-m-long, 33.5-m-wide and 3-m-deep lock could be filled with water at 4°C within a period of about 18.5 hr. Stratification of water somewhat complicates estimates of the requisite discharge to keep lock water at or above 0°C. Analytically the estimation involves a nonlinear problem insofar as thermal conduction from a deepening, warmer, lower layer of water becomes increasingly important. Basic equations associated with thermal-energy conservation for this condition are presented in Appendix B. Before expending effort in solving this problem, it is pertinent to consider the practicality of providing sufficient discharge of groundwater. Certain concerns to be considered are as follows:

1. Magnitude of discharge. As indicated in Table 3, if T_g = 5.6°C, some 0.078–0.105 m^3/s of groundwater discharge would be required when air temperatures were –15 to –20°C. This demand is approximately equivalent to that for a community of 10,000 people each consuming on the average of 0.76 m^3/day. If T_g = 12.2°C the water demand would be about 0.036–0.048 m^3/s for the same condition.

2. Adequacy of groundwater supply. Sufficient aquifer capacity is required to sustain the requisite discharge of groundwater. It is likely that, at many lock sites, groundwater-recovery wells would be placed near a river such that a significant proportion of groundwater would indirectly be river water. A consequence of this could be that the groundwater temperature may be somewhat lower than 5.6°C or 12.2°C. If groundwater is not recharged with river water, consideration needs to

Table 3. Required groundwater discharge to maintain lock water at 0°C. (From information provided by G.D. Ashton 1985.)

Air temp T_a *(°C)*	*Power loss to air* ϕ_{wa} *(mW)*	*Groundwater discharge Q* (m^3/s) $T_g = 5.6°C$	(m^3/s) $T_g = 12.2°C$
–5	0.61	0.0262	0.0121
–10	1.23	0.0523	0.0241
–15	1.86	0.0785	0.0361
–20	2.45	0.1045	0.0480
–25	3.06	0.1306	0.0600

Note: 1 mW = 10^6 W = 1340 horsepower.

be given to the effect of groundwater removal on water-table elevation.

3. Mixing of lock water. To appreciate the mixing difficulty, it is useful to visualize a discharge of 0.078 m^3/s into a lock: picture, say, two water jets issuing from 0.20-m-diameter nozzles at a mean velocity of 1.3 m/s; each jet would penetrate about 20 m before the mean jet velocity diminishes to about 0.15 m/s. If mixing is assessed in terms of a densimetric Froude number F_d [= $V/(gy\Delta\rho/\rho)^{1/2}$] associated with water flow through a lock, with the mean flow velocity being (0.078 m^3/s)/(10 m × 33.5 m) and the normalized density difference $\Delta\rho/\rho$ taken as 10^{-4}, it becomes evident that the lock water is not well mixed; F_d is on the order of 10^{-3}. Consequently additional mixing would be needed to ensure that heat released from groundwater is rapidly dispersed to the surface area of the lock. If a manifold comprising many smaller-diameter nozzles (for example, 25-mm in diameter) is considered, concern may arise as to the freezing of the flowing water in these nozzles.

4. Throughflow in the lock. The groundwater discharge requirements summarized in Table 3 were obtained under the assumption that river water does not flow through the lock. However, at two lock and dam installations visited, it was reported that it is fairly common during winter to have lock miter gates slightly ajar, allowing some throughflow of water to inhibit ice growth within the central portion of the lock.

Water at 12.2°C is less dense than at 0°C. Consequently it is more readily retained at the surface of a lock chamber than is water at 4°C, at least until it is cooled to 4°C. However, the four concerns enumerated above still need to be taken into account. The crucial concern is in assuming that the groundwater becomes uniformly and rapidly distributed over most of the lock chamber. The power requirements to pump and mix groundwater within a lock chamber should be assessed for comparison with power applied for direct heating of lock walls as an alternative approach. Consider a system comprising two 0.063-m^3/s, 30.5-m head pumps for pumping groundwater, and two 0.063-m^3/s, 15.2-m-head pumps for dispersing groundwater throughout a lock chamber. The power requirements, allowing for pump efficiency, would be about 60 kW for the former and 38 kW for the latter, a total power of 98 kW. This example is approximate and possibly conservative, but it illustrates the potential power requirements.

Power to heat water near lock walls

An alternative to heating the entire body of water contained in a lock is to heat water in the vicinity of the lock walls at the elevation where ice collars predominantly form. To do this, a manifold would be needed to distribute groundwater flow (or heat) along the wall, and ideally to instigate a flow circulation, as illustrated in Figure 15. Two criteria need to be considered in assessing the requisite groundwater discharge to maintain water at or above 0°C in a strip of width B along a lock wall:

- Thermal power derived from groundwater discharge should balance the rate of heat loss to air; and
- The manifold discharge should be of sufficient magnitude that manifold jets adequately mix the water in the strip.

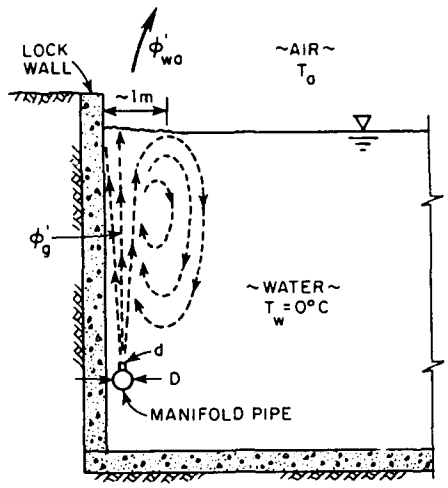

Figure 15. Heat transfer and warm water circulation near a lock wall.

The rate of heat loss to air from strips of width W' along both lock walls can be expressed as

$$\phi'_{wa} = 2H'_{wa}(T_w - T_a)LW'. \quad (5)$$

If the heat transfer coefficient H'_{wa} = 20 $W/m^2 \cdot °C$, W' = 1 m, L = 183 m and T_w = 0°C, then eq 5 yields values of ϕ'_{wa}, for varying T_a, as summarized in Table 4. These values of ϕ'_{wa}, which are $2W'/W$ (= 2 × 1/33.5 = 0.06)

Table 4. Heat loss rate and groundwater discharge at strips bordering lock walls.

Air temp T_a (°C)	*Power loss to air* ϕ_{wa} (mW)	*Groundwater discharge Q* (m^3/s) T_g = 5.6°C	T_g = 12.2°C
-5	37	0.0016	0.0007
-15	110	0.0047	0.0021
-25	183	0.0078	0.0036

Notes:
1 kW = 10^3 W = 1.34 horsepower.
Calculation was made for the assumed surface area to be heated directly: 2 × 183 m × 1 m = 366 m^2.

times the ϕ_{wa} values listed in Table 3, have to be balanced by heat released from groundwater discharge along the lock walls. The requisite groundwater discharge would be

$$Q = \phi'_{wa} / [\rho_w c_p (T_g - T_w)]. \quad (6)$$

Table 4 lists values of Q commensurate with $T_g = 5.6$ and 12.2°C for a range of T_a values. The requisite values of Q are comparatively modest. They are, however, insufficient to mix the water along the lock walls.

Consider now the discharge requirements for a water-jet manifold placed along a lock wall so as to release "warm" water and to create a desirable level of turbulence at the water surface. To estimate the discharge requirements, the manifold geometry depicted in Figure 16 is assumed, together with the following design criteria:

- The maximum velocity at the water surface, located at height h above manifold nozzles, is 0.3 m/s;
- The strip affected by the circulation cell generated by each water jet is 1 m wide; and
- The nozzles are 0.01 m in diameter and are spaced 2 m apart along a 180-m-long manifold pipe. If it is assumed that the total outlet area should not exceed about one third of the manifold area, a 0.25- or 0.30-m-diameter manifold pipe would be required.

If each nozzle flow is treated as a circular turbulent jet and the density difference between the jet water and the lock water is neglected, the following relationships may be used to estimate jet and manifold discharges (Rajaratham 1976):

$$V_m/V_o = 6.3\,(d/h) \quad (7)$$

$$B_j = 0.10\,h \quad (8)$$

and

$$Q/Q_o = 0.32\,(h/d) \quad (9)$$

where V_o = jet velocity at the nozzle
V_m = maximum jet velocity at elevation h above the nozzle
d = nozzle diameter
B_j = jet width at elevation h above the nozzle
Q_o = nozzle discharge
Q = nozzle discharge plus entrained discharge.

Using $V_m = 0.3$ m/s at, for example, $h = 3$ m and $d = 0.025$ m yields $V_o = 5.7$ m/s, $B_j = 0.3$ m, $Q_o = 2.8 \times 10^{-3}$ m^3/s and $Q = 0.108$ m^3/s. The total discharge through a manifold placed along each lock wall would be approximately 0.151 m^3/s. Evidently much greater discharges are required for mixing than for heating. If mixing is assessed in terms of a representative densimetric Froude number F_d for flow through a lock, it becomes evident that lock water is marginally well mixed; F_d is on the order of unity.

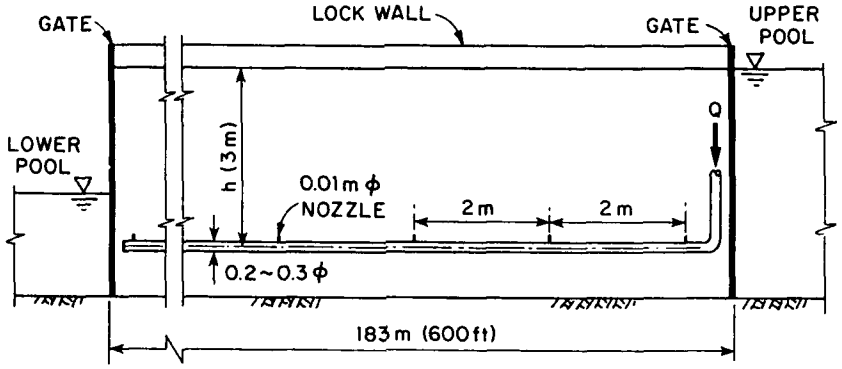

Figure 16. Manifold dimensions for an assumed diffuser pipe.

If groundwater at 5.6°C is added at, say, 0.0032 m^3/s with river water pumped at 0°C and 0.151 m^3/s before being passed through each manifold, the blended flow would have a temperature of about 0.1°C. If the groundwater is at 12.2°C, the blended flow would have a temperature of about 0.25°C. The blended discharge may be adequate to maintain an ice-free strip along each lock wall, but practical difficulties may arise:

- The blended flow may cool to 0°C when conveyed along the manifold;
- If the water surface is located at an elevation greater than 3 m above the manifold, greater water discharges would be needed;
- A 0.25- to 0.30-m-diameter pipe may itself be an unacceptable protrusion into the lock; and
- The manifold would have to be designed such that it can be quickly drained when exposed to frigid air when the water level in the lock is lowered.

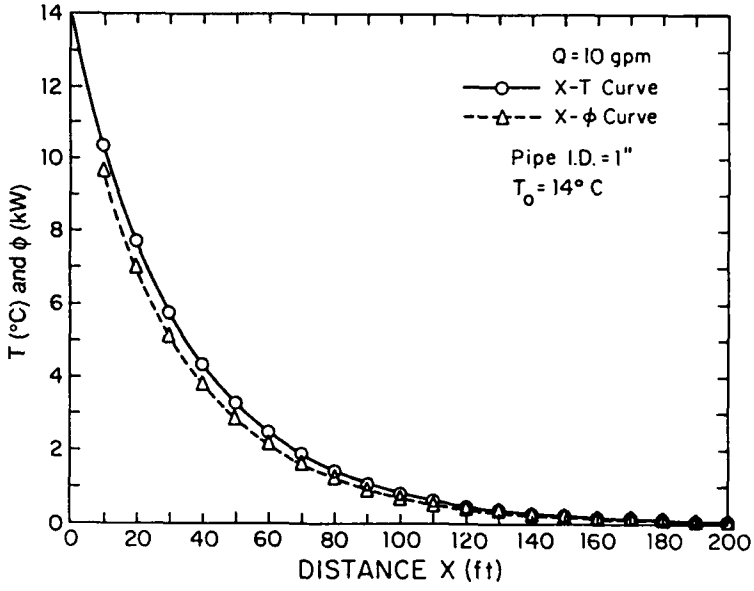

Figure 17. Heat transfer characteristics of pipe flow (Q = 10 gal./min).

Heat-transfer characteristics of piped flow in lock walls

Another means of using warm groundwater energy would be to circulate it through pipes embedded in lock walls or through pipes placed in special tubes located in lock walls. The convective heat transfer from flow through a pipe placed in a concrete lock wall can be estimated in the following manner.

Consider a steady flow through a pipe with a constant pipe-wall temperature T_o. The temperature distribution along the flow direction x is (Welty 1978)

$$(T - T_o) / (T_e - T_o) = e^{-St(4x/D)} \qquad (10)$$

where T = water temperature at x (°C)
T_e = entrance water temperature at $x = 0$ (°C)
St = Stanton number
x = longitudinal distance (m)
D = pipe diameter (m).

An empirical relationship for the Stanton number developed by Colburn (1933) is

$$St = 0.023\, Re^{-0.2}\, Pr^{-2/3} \qquad (11)$$

where Re is the Reynolds number evaluated at the film temperature, which is defined as the average of entrance and exit temperatures, and Pr is the Prandtl number evaluated at the film temperature. T_L, the exit temperature at $x = L$, must be determined from eq 10 and 11 by a trial-and-error procedure because the film temperature cannot be predetermined. The exit temperature is first assumed, and Re and Pr are subsequently determined. The Stanton number given by eq 11 is then substituted into eq 10 to obtain T_L. If this exit temperature is not close to the assumed value, the same procedure is repeated with a new T_L until the agreement is satisfactory. Once T_L is determined, the heat transfer ϕ can be obtained according to

$$\phi = \rho_w [AVc_p(T_L - T_e)] \qquad (12)$$

where ρ_w = density of water (kg/m^3)
A = pipe cross-section area (m^2)
V = average flow velocity (m/s)
c_p = specific heat of water (W·s/kg·°C).

Following the general procedure outlined above, several practical cases in which the pipe-wall temperature T_o was kept at 0°C were examined. Figure 17 shows the computed results of temperature and heat-transfer variations along the x direction in which $D = 0.025$ m, $T_e = 14$°C, $Q = 6.3 \times 10^{-4}$ m^3/s and $V = 1.24$ m/s. As can be seen in Figure 17, the water temperature drops very rapidly along the flow direction and reaches the freezing point within about $x = 200$ ft. The heat transferred to the lock wall from warm-water pipe flow was also estimated at 10-ft intervals, and its spatial distribution is shown in the same figure. Because the power ϕ is proportional to the temperature difference $T_L - T_e$, it decreases with water temperature. The total heat transferred in this 61-m-long pipe segment is the sum of ϕ shown in the figure, which amounts to about 37 kW. Figure 18 shows the computed results for a similar case with a different discharge of 9.5×10^{-4} m^3/s. Figure 19 depicts the case of $Q = 2.5 \times 10^{-3}$ m^3/s, $D = 0.050$ m and $V = 1.24$ m/s. The water temperature decreases rather rapidly: $T = 7.3$°C at $x = 15.2$ m, $T = 3.9$°C at $x = 30.5$ m, $T = 2.1$°C at $x = 45.7$ m and $T = 1.2$°C at $x = 61$ m.

The total power expended along a 61-m-long pipe

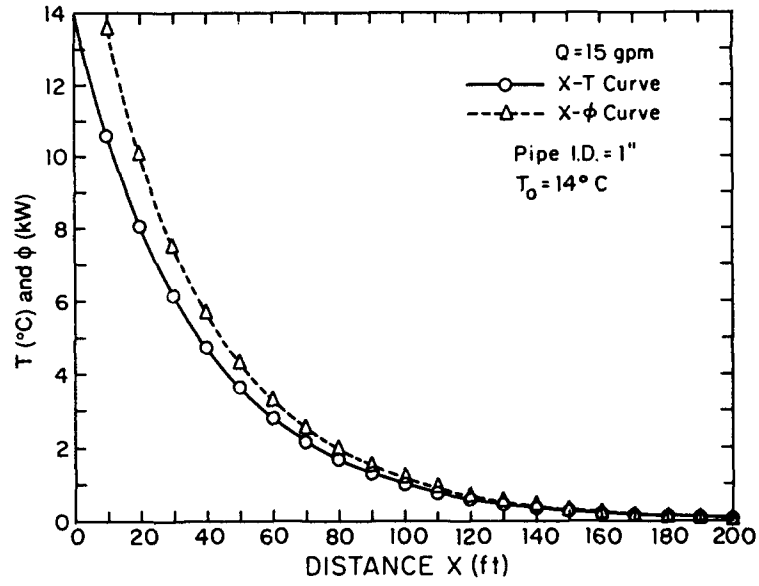

Figure 18. Heat transfer characteristics of pipe flow (Q = 15 gal./min).

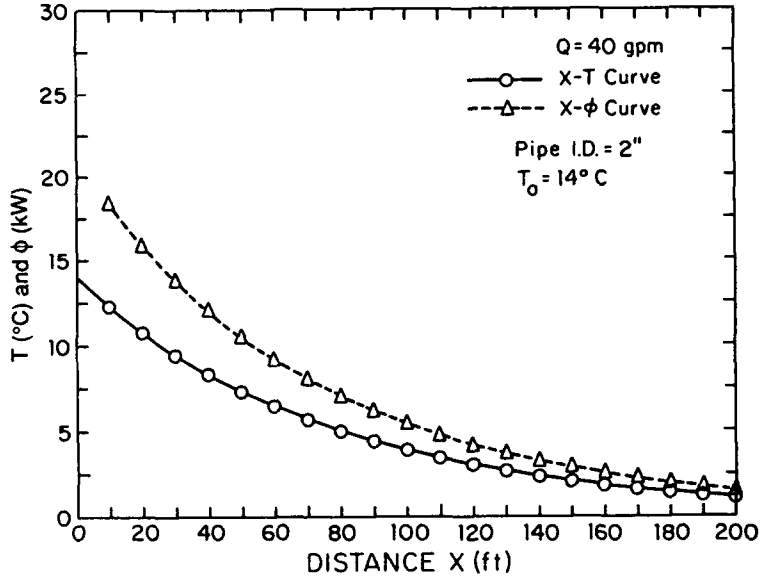

Figure 19. Heat transfer characteristics of pipe flow (Q = 40 gal./min).

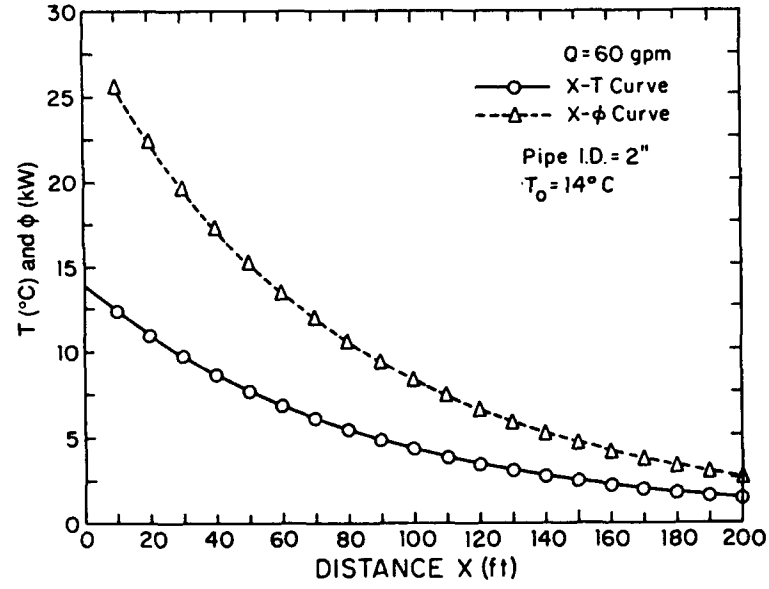

Figure 20. Heat transfer characteristics of pipe flow (Q = 60 gal./min).

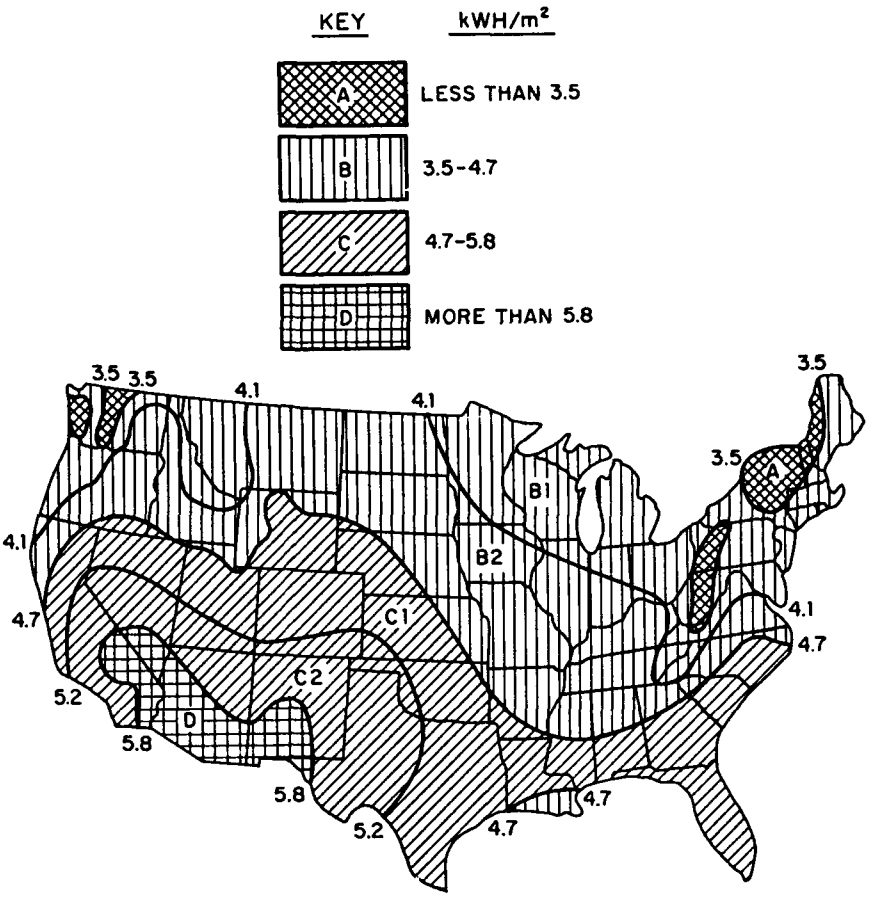

Figure 21. Distribution of mean daily solar radiation in the United States. (After Katzman 1983.)

section is about 136 kW. When the water discharge is increased by 50% ($Q = 0.0038$ m^3/s), the water temperature at $x = 61$ m is estimated to be about 1.4°C (Fig. 20), and the total power expenditure is about 200 kW. From these examples, it is clear that unless extremely high temperature water (or steam) is passed through small pipes embedded in lock walls, the water temperature reaches the freezing point very rapidly without traveling too far if the lock wall temperature is below the freezing point. In conclusion, heating lock walls by means of small pipes carrying groundwater is not practical.

Before determining the means of overcoming these difficulties, groundwater use should be compared with other alternative heating methods, such as heating cables and steam pipes embedded in lock walls. Alternatively, agitation of flow along lock walls alone may be sufficient to significantly reduce ice-collar growth. River water pumped from the upper pool could also be passed through a manifold pipe located near the base of each lock wall. An advantage of using river water is that it is easily accessible and would not require large-power pumps to circulate it through a manifold.

Solar energy

Although solar energy is abundant, even in the northern part of the U.S., applying solar energy to keep lock and dam installations ice-free during winter does not seem to be practical. As can be seen in Figure 21, approximately 4 kWh/m^2 of mean solar energy is available daily in most northern midwest and northeast parts of the U.S. in winter. To put this in context, consider a small house with a south-facing roof area of about 100 m^2. It receives about 400 kWh of solar energy every day, or 12,000 kWh per month, which is far greater than a household's average monthly electric use of 1000 kWh. Therefore, theoretically speaking, only a 10% efficiency rate in capturing this solar energy is adequate to meet residential electric demands. However, this level of solar energy is available only during clear daylight conditions, which seldom prevail in the northern U.S. because cloudy days prevail during most of the winter. As a practical matter, it should be kept in mind that thermal energy for ice control is particularly needed during nights when solar radiation is not available: thus, air temperature drops sharply.

To demonstrate the efficiency of solar-energy col-

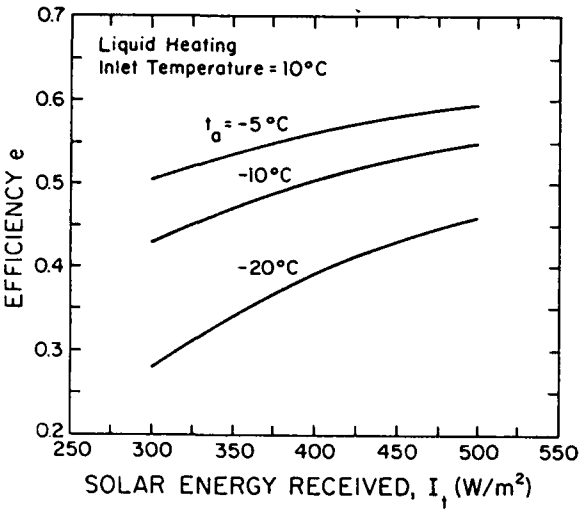

Figure 22. Efficiency of liquid solar collector.

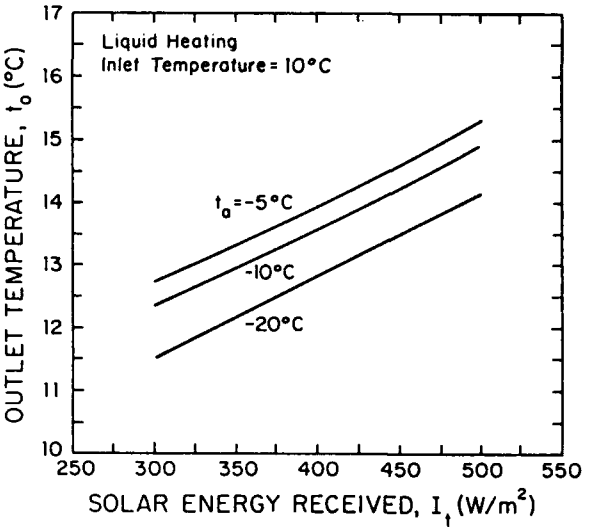

Figure 23. Outlet temperature of liquid solar collector.

lectors, a sample evaluation was made for a typical, standard liquid heater (2 × 1 × 0.15 m) with a steel absorber, single-glazed glass and 50-mm-thick back insulation (Dickinson and Cheremisinoff 1980). The efficiency of a solar collector e can be determined from

$$e = F_R t_r a - F_R H_s (t_i - t_a)/I_t \qquad (13)$$

where F_R = heat removal factor
t_r = transmissivity (the fraction of the incoming solar radiation that reaches the absorbing surface)
a = absorptivity (the fraction of solar energy reaching the surface that is absorbed)
H_s = overall heat-loss coefficient
t_i = liquid inlet temperature
t_a = air temperature
I_t = solar energy received on the upper surface of the sloping collector surface.

If we assume that $F_R t_i a$ = 0.73 and $F_R H_s$ = 4.49 W/m^2·°C (Dickinson and Cheremisinoff 1980), the efficiency e can be estimated using eq 13 for various combinations of t_i, t_a and I_t. Table 5 summarizes the computed efficiency for three air temperatures (–5, –10 and –20°C) for a range of I_t from 300 to 500 W/m^2, which is typical around noon in Minneapolis, Minnesota, which is at a latitude of 45°N. We assume in this estimation that warm groundwater at 10°C is available as a liquid to absorb solar energy. The results for efficiency are also depicted in Figure 22. The efficiency decreases very rapidly as air temperature decreases because heat loss is directly proportional to the temperature difference between liquid and air according to eq 13. Using the estimated efficiency, we estimated the liquid outlet temperature t_o for each case (Table 5, Fig. 23). As can be seen in Figure 23, the temperature rise gained by means of a liquid solar collector is at most 5°C for a range of air temperature from –5 to –20°C.

Wind energy

Wind energy is not reliably available over time,

Table 5. Computed efficiency and outlet temperature of liquid solar collector.

Solar radiation I_t	*Efficiency* e			*Outlet temperature* t_o *(°C)*		
(W/m²)	t_a = –5°C	–10°C	–20°C	t_a = –5°C	–10°C	–20°C
300	0.505	0.430	0.280	12.72	12.34	11.51
400	0.562	0.506	0.393	13.95	13.55	12.82
500	0.595	0.550	0.460	15.31	14.92	14.15

Design parameters:
$F_R t_r a$ = 0.73.
$F_R H_s$ = 4.49 (W/m^2·°C).
Water discharge = 0.0136 (kg/m^2·s).
Specific heat of water = 4.2 (kJ/kg·°C).

Notes:
F_R = heat removal factor.
t_r = solar radiation transmissivity.
a = solar radiation absorptivity.
H_s = overall heat-loss coefficient.

although daily and annual cycles of average wind speed are surprisingly stable from year to year. The power output of a horizontal windmill strongly depends on wind speed (Dickinson and Cheremisinoff 1980):

$$P = 0.5\, e\, \rho A V^3 \qquad (14)$$

where P = power output (W)
e = efficiency
ρ = air density = 1.293 kg/m^3 at 0°C, 1 atmosphere and sea level
A = area of the rotating components (m^2)
V = wind speed (m/s).

Wind speeds can change by 50% from one hour to the next, and gusting may alter wind speeds by a factor of three or more in a matter of seconds. From eq 14 it is clear that power varies as the cube of the wind speed, which means that a change in wind speed by a factor of two, for example, can result in a change in power output by a factor of eight. It is not surprising, therefore, that there are practical engineering problems to be overcome in the area of system control, such that variable electrical energy output can be converted to constant-frequency AC that is phased synchronously with a utility network.

Consider the wind-power equation given by eq 14 to estimate the power output that can be generated near Pittsburgh, Pennsylvania, or Minneapolis, Minnesota. In these areas the average winter wind speed is about 4 m/s (Pierson 1978). A windmill with 6-m-diameter rotor blades (area = 28.27 m^2) and an efficiency of 0.5 can generate electric power output P as

$$P = 0.5 \times 0.5 \times 1.293 \times 28.27 \times 43 = 585 \text{ W}. \qquad (15)$$

This means that at least four or five 6-m-diameter windmill units are needed to supply 2.5 kW to even one unit of the quartz heaters described earlier. Therefore, wind energy does not appear to be feasible for supplying power for ice control in navigation locks and dams.

Hydroelectric energy

Although hydroelectric energy is usually thought of as a conventional energy source, it is included in this study because it could be generated in unconventional ways at many lock and dam installations. Microhydroelectric power plants can be found at several navigation lock and dam installations, such as L&D No. 15 on the Mississippi River, with a generator rated at 312 kW at 3.7-m gross head; L&D No. 3 on the Allegheny River, with a 60-kW unit at 4.1-m gross head; and Emsworth L&D on the Ohio River, with a 300-kW unit at 5.5-m gross head. Electric power generated in these installations has been used primarily to operate lock and dam gates and for general maintenance purposes.

Locks and dams are primarily constructed to regulate the stages of rivers for navigation. The pools that they create, however, can provide significant hydraulic heads, which can be used for hydropower generation. The capability to fully exploit low-head hydropower has, until recently, been ignored, mainly because most available turbines were developed for relatively high heads. However, so-called "low-head" microhydropower plants have been built since the late 1970s at many existing low-head dams in the U.S., and many more projects are pending. Before discussing the feasibility of microhydropower plants for ice control, consider first the hydropower output relationship.

The hydroelectric power output P is generally expressed as

$$P = 9.8\, eQH \qquad (Q \text{ and } H \text{ in SI units}) \qquad (16a)$$

or

$$P = 0.0847\, eQH \quad (Q \text{ and } H \text{ in English units}) \qquad (16b)$$

where P = power output (kW)
e = efficiency
Q = water discharge (m^3/s in eq 16a; ft^3/s in eq 16b)
H = net head (m in eq 16a; ft in eq 16b).

The power output, therefore, can be estimated using eq 16 for various combinations of water discharge and head, as summarized in Table 6. The estimated outputs shown in Table 6 were obtained by assuming that the output efficiency is 0.8.

Table 6 can be used to evaluate the feasibility of a microhydropower plant at existing lock and dam instal-

Table 6. Hydroelectric power output for various water discharge–head combinations.

Water discharge, Q	P *(kW)*			
(m^3/s)	*H = 1.5 m*	*3.1 m*	*4.6 m*	*6.1 m*
7.1	85	170	255	340
14.2	170	340	510	680
21.2	255	510	760	1015
28.3	340	680	1015	1355
34.1	425	845	1270	1695
42.5	510	1015	1525	2035
49.6	595	1185	1780	2370
56.6	680	1355	203	2710

Notes:
P (kW) = 9.8 × e × Q (m^3/s) × H (m).
e = efficiency (assumed to be 0.8).
Q = water discharge.
H = net head.

lations. Consider, for example, L&D No. 5 on the Mississippi River, which requires about 140 kW of power to de-ice six roller gates by means of quartz heaters and side-seal heaters, as described earlier. Because a net head of about 2.1 m is available at L&D No. 5, only about 8.4 m^3/s of discharge is sufficient in generating this amount of power. Another example shows that if a discharge of 14.2 m^3/s is available at a net head of 3 m, as much as 340 kW of power output can be generated (Table 6). This is more than the power required for heating two 183-m-long and 2-m-high lock walls to control ice-collar growth (approximately 300 kW), which was estimated under the assumed conditions of a heat-loss coefficient of 20 $W/m^2 \cdot °C$, a lock-wall surface temperature of 0°C and an air temperature of –20°C. Eranti et al. (1983) reported similar estimates on the heat energy required to maintain satisfactory operation of lock facilities along the Saimaa Canal in Finland. According to their analysis, approximately 300 kW of thermal energy is needed for each lock.

Although unconventional energy sources may be cheaper than conventional sources, such as power supplied by commercial utilities, a crucial question to be addressed is: how can the requisite level of hydroelectric energy be generated without extensive, and expensive, modifications of existing lock and dam installations? Although the Power Barge™ concept by Broome (1985, 1987) is still in its demonstration stages, a prefabricated, portable power plant appears to offer an extremely advantageous, and inexpensive, means to generate hydropower for use in ice control. There are two prototype demonstration projects pending: a 500-kW unit at a net head of 5.5 m and discharge of 11.3 m^3/s (Broome 1985), and a 1250-kW unit at a net head of 3.7 m and discharge of 42.5 m^3/s (Broome 1987). The portable power plant comprises an anchored upstream barge (which provides the water intake), a siphon penstock and a downstream barge (which houses a submersible horizontal turbine). The design employs trunnion-type joints to accommodate variations in head. Because no major construction is involved, it appears to produce minimal environmental impacts. Unlike conventional, shore-attached power plants, it can be placed at any location along the dam, permitting a downstream flow distribution favorable to overall navigation and aquatic environments. This unconventional means of generating hydropower energy seems to be particularly well suited for low-head lock and dam installations.

CONCLUSIONS

The principal conclusions derived from this investigation are as follows:

1. At lock and dam installations the primary ice growths of concern, and to be controlled by heat application, are ice-collar formation along lock walls, and dam gates frozen to upstream ice sheets and encrusted by icings from water splash, spray and seepage.

2. The level of power required to inhibit ice growth along two walls (183 m long and 2 m high) of a standard lock chamber is on the order of 300 kW when the air temperature is about –20°C, the coefficient of heat transfer from lock wall to frigid air is taken as 20 $W/m^2 \cdot °C$, and the lock walls are heated to 0°C. This power requirement, which is equivalent to about 400 W/m^2, is reduced proportionately with higher air temperatures. It can be reduced further if lock wall sections are heated consecutively, rather than all of the walls heated at the same time. Still further reductions in power are possible if heat is applied intermittently to dislodge ice grown on lock walls rather than to prevent ice growth.

3. Experience with typical lock and dam installations, notably L&D No. 5 and 6 on the Mississippi River, indicates that, during typical winters, roller and tainter gates can be maintained operable by means of four quartz heaters (powered at 10 kW total) and two side-seal heaters (powered at 13.8 kW total). Therefore, an approximate total of 24 kW is required to keep one gate operable. A dam comprising ten gates, all kept operable during winter, would require about 240 kW for simultaneous heating, with proportionately less power needed if fewer gates are heated.

4. The most attractive unconventional energy source that meets the power requirements appears to be hydroelectric power generated at locks and dams by means of small, portable, power-barge plants. A single plant can generate 300 kW, for example, at a net head of about 3 m and a water discharge of about 13 m^3/s. It is recommended that the prototype power-barge projects be closely monitored and a more detailed feasibility study, including an economic analysis, be undertaken.

5. Direct heating of lock walls, lock miter-gate recesses, and dam-gate pier walls by means of electrical heaters embedded in concrete walls is the best approach for controlling ice growth on lock walls and dam gates.

6. Neither solar energy nor wind energy is feasible for ice control at lock and dam installations because they are unreliable, since no solar power is generated during nights and no wind power is generated during windless days.

7. The use of groundwater to control ice formation in locks seems attractive. However, the practical aspects of mixing groundwater with lock water, or discharging it along lock walls, diminish its general utility for ice control. Additionally, as the groundwater temperature decreases with increasing latitude, so does the attractiveness of its use for ice control. The analysis of heating

water near lock walls also shows that a greater amount of discharge would be required for mixing than for heating water along each lock wall. It is not feasible to use warm groundwater by passing it through pipes embedded in lock walls for maintaining lock walls ice-free.

LITERATURE CITED

Balanin, V., G. Vasiliev and V. Smirnov (1986) Rational design of lock mechanical devices operating under ice conditions. In *Proceedings of the IAHR Ice Symposium, Iowa City, Iowa*, vol. 3, p. 307–321.

Broome, K.R. (1985) The power barge hydroelectric plant design concept. In *Proceedings of ASCE, Waterpower '85 Convention, Detroit, Michigan.*

Broome, K.R. (1987) The Power Barge™ demonstration project at Chain Dam. In *Proceedings of ASCE, Waterpower '87 Convention, Portland, Oregon.*

Carslaw, H.S. and J.C. Jaeger (1947) *Conduction of Heat in Solids*. Oxford: Clarendon Press.

Colburn, A.P. (1933) A method of correlating forced convection heat transfer data and a comparison with fluid friction. *Transactions, AIChE*, **29**: 174.

Dickinson, W.C. and P.N. Cheremisinoff (Ed.) (1980) *Solar Energy Technology Handbook, Part A; Engineering Fundamentals*. New York: Marcell Dekker.

Eranti, E., M. Pentinnen and T. Rokonen (1983) Extending the ice navigation season in the Saimaa Canal. In *Proceedings of the 7th International Conference on Port and Ocean Engineering Under Arctic Conditions, Helsinki, Finland*, vol. 1, p. 381–391.

Frankenstein, G. and C.A. Wortley (1984) Methods of ice control for winter navigation in inland waters. In *Proceedings of the IAHR Ice Symposium, Hamburg, West Germany*, vol. 1, p. 329–337.

Johnson, E.E., Inc. (1966) *Groundwater and Wells—A Reference Book for the Water-Well Industry*. St. Paul, Minnesota: Edward E. Johnson.

Katzman, M.T. (1983) *Solar and Wind Energy; An Economic Evaluation of Current and Future Technology*. Totawa, New Jersey: Rowman and Allanheld Publishers.

Pierson, R.E. (1978) *Technician's and Experimenter's Guide to Using Sun, Wind, and Water Power*. West Nyack, New York: Parker Publishing Company.

Rajaratham, N. (1976) Turbulent jets. In *Developments in Water Science*. New York: Elsevier Scientific Publishing Company, vol. 5.

Thomas, J.A. (1976) Heating of lockwalls for prevention of ice formation. St. Lawrence Seaway Authority Engineering Service Branch, Project No. E1.074, File No. 60-24-1-1.

Welty, J.R. (1978) *Engineering Heat Transfer*. New York: John Wiley and Sons.

Zufelt, J. and D. Calkins (1985) Summary of ice problem areas in navigable waterways. USA Cold Regions Research and Engineering Laboratory, Special Report 85-2.

APPENDIX A: MATHEMATICAL ANALYSIS OF HEAT-TRANSFER PROCESSES THROUGH NAVIGATION LOCK WALLS

ONE-DIMENSIONAL HEAT-DIFFUSION MODEL

Because the heat conductivity of concrete is extremely low (approximately two orders of magnitude smaller than that of metal), the use of an isolated heating rod in a two-dimensional field as a point source is not effective in heating a long lock wall. Therefore, a one-dimensional heat-transfer model with a continuous plane heat source along the lock wall was first evaluated.

Consider a continuous, steady heat source embedded in concrete along a lock wall, as shown in Figure A1. The governing equation for a one-dimensional heat diffusion is

$$\frac{\partial \theta}{\partial t} = k \frac{\partial^2 \theta}{\partial x^2} \tag{A1}$$

where θ = temperature (°C)
k = heat diffusivity (m^2/s)
x = distance (m)
t = time (s).

If heat is liberated at the rate of $\rho c_p q$ (W/m^2) per unit area per unit time in the plane $x = x'$ at time $t = 0$, a general solution of eq A1 is

$$\theta = q\left\{(t/\pi k)^{1/2} \exp\left[-\frac{(x-x')^2}{4kt}\right] - \frac{|x-x'|}{2k}\operatorname{erfc}\left(\frac{|x-x'|}{2\sqrt{kt}}\right)\right\} = E(x-x') \tag{A2}$$

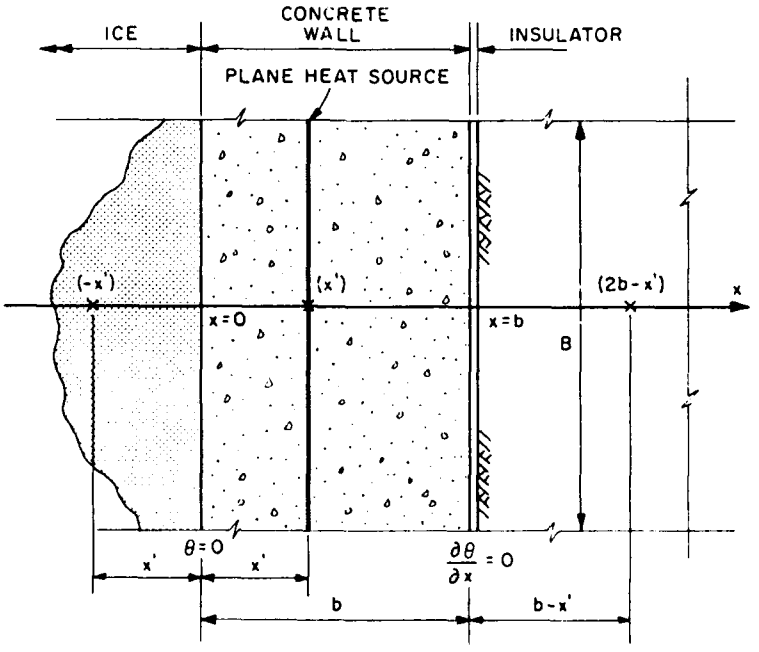

Figure A1. Definition sketch of plane heat-source model.

where q = heat-source strength (°C·m/s)
ρ = density of solid (kg/m^3)
c_p = specific heat of solid (W·s/kg·°C)
E = function expressing temperature distribution when the heat source is placed at $x = x'$.

If the temperature of the lock wall surface is assumed to be 0°C due to ice attached to the lock wall, and a heat insulator is placed at $x = b$, as shown in Figure A1, the boundary conditions become

$$\left.\begin{aligned} &\theta = 0°C && \text{at } x = 0 \ (t > 0) \\ &\text{and} \\ &\frac{\partial \theta}{\partial x} = 0 && \text{at } x = b \ (t > 0). \end{aligned}\right\} \tag{A3}$$

To satisfy eq 3 it is necessary to superimpose a plane sink at $x = -x'$ and a plane source at ($x = 2$) ($b - x'$), which yields the following temperature distribution:

$$\theta = E(x - x') - E(x + x') + E(x + x' - 2b). \tag{A4}$$

It is more convenient, for the purpose of generalizing the analysis, to use the following normalized variables:

$$\left.\begin{aligned} X &= x/b \\ X' &= x'/b \\ T &= kt/b^2. \end{aligned}\right\} \tag{A5}$$

Normalized temperature θ, corresponding to eq A2, can be written as

$$\Theta = \frac{\theta}{q(b/k)} = \sqrt{\frac{T}{\pi}} \exp\left[-\frac{(X-X')^2}{4T}\right] - \frac{|X-X'|}{2} \operatorname{erfc}\left(\frac{|X-X'|}{2\sqrt{T}}\right). \tag{A2a}$$

Similarly, eq A4 becomes

$$\begin{aligned} \Theta = \frac{\theta}{q(b/k)} &= \sqrt{\frac{T}{\pi}} \exp\left[-\frac{(X-X')^2}{4T}\right] - \frac{|X-X'|}{2} \operatorname{erfc}\left(\frac{|X-X'|}{2\sqrt{T}}\right) \\ &- \sqrt{\frac{T}{\pi}} \exp\left[-\frac{(X+X')^2}{4T}\right] + \frac{|X+X'|}{2} \operatorname{erfc}\left(\frac{|X+X'|}{2\sqrt{T}}\right) \\ &+ \sqrt{\frac{T}{\pi}} \exp\left[-\frac{(X+X'-2)^2}{4T}\right] - \frac{|X+X'-2|}{2} \operatorname{erfc}\left(\frac{|X+X'-2|}{2\sqrt{T}}\right). \end{aligned} \tag{A4a}$$

Temporal variations of θ, as predicted using eq A4a, are shown in Figures A2 and A3 for two plane-source positions: $X' = 0.25$ and 0.50, respectively. The information in Figures A2 and

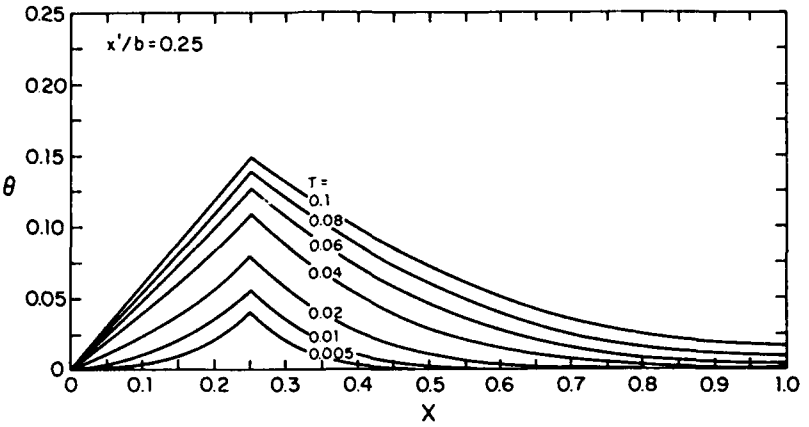

Figure A2. Spatial distributions of normalized temperature in one-dimensional model (x′/b = 0.25).

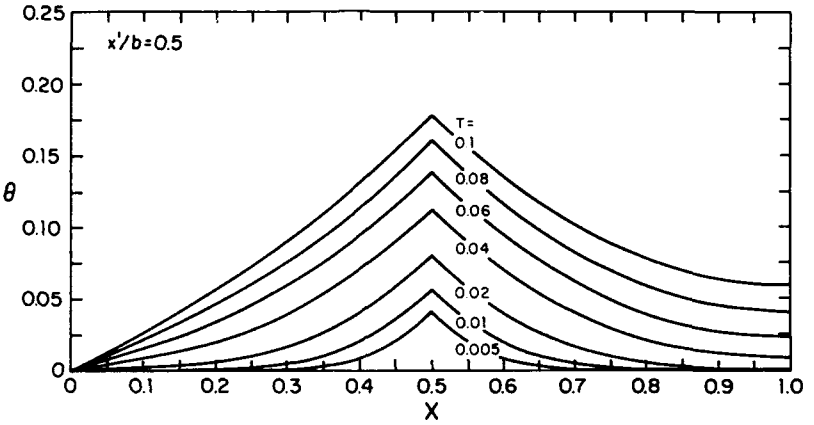

Figure A3. Spatial distributions of normalized temperature in one-dimensional model (x′/b = 0.5)

A3 can be used to estimate power requirements for keeping a lock wall ice-free. Taking the height of the zone of ice formation on a lock wall of length B to be H, and the power supplied to the plane source Q, the requisite heat strength q to maintain ice-free conditions over the wall is

$$q = \frac{Q}{\rho c_p BH} \tag{A5}$$

and

$$\Theta = \frac{\theta}{\left(\frac{Qb}{KBH}\right)} \tag{A6}$$

where K is the thermal conductivity ($\rho c_p k$) in W/m·°C.

Consider a lock wall under the following conditions: B = 250 m, H = 2 m, b = 0.30 m, k (concrete wall) = 4.2×10^{-7} m^2/s, x' = 0.075 m and Q = 250 kW. The approximate temperature at x = 0.03 m when t = 2.4 hours can be obtained as follows:

Normalized heat-source location: $X' = x/b = 0.075/0.30 = 0.25$

Normalized time: $T = \frac{kt}{b^2} = \frac{4.2 \times 10^{-7} \times 2.4 \times 3600}{0.3^2} = 0.04$

Normalized location: $X = x/b = 0.03/0.30 = 0.10$

Normalized temperature: $\theta = 0.038$ (from Figure A2).

Thus, the actual temperature θ is

$$\theta = \frac{\Theta bQ}{KBH} = \frac{0.038\ [0.03\ (\text{m})]\ [250 \times 10^3\ (\text{W})]}{[0.85\ (\text{W/m} \cdot °\text{C})]\ [250\ (\text{m})]\ [2\ (\text{m})]} = 6.7°\text{C}.$$

The power per unit area of wall H_f associated with heat transferred from the concrete surface to balance ice formation at the lock wall ($x = 0$) is then

$$H_f = -K \frac{\partial \theta}{\partial x} \left(\text{W/m}^2\right). \tag{A7}$$

Therefore, the total heat transfer H_{ft} in time t can be determined as

$$H_{ft} = \int_0^t \left(-K \frac{\partial \theta}{\partial x}\right) d\tau \left(\text{W·hr/m}^2\right) \tag{A8}$$

which can be normalized as

$$\overline{H}_{ft} = \frac{H_{ft}}{\left(\frac{Q}{BH}\right)\left(\frac{b^2}{k}\right)} = -\int_0^T \left(\frac{\partial \Theta}{\partial x}\right) dT. \tag{A9}$$

Figure A4 shows $\overline{H}_{ft}$ plotted as a function of T for the case of a heating plate placed in the

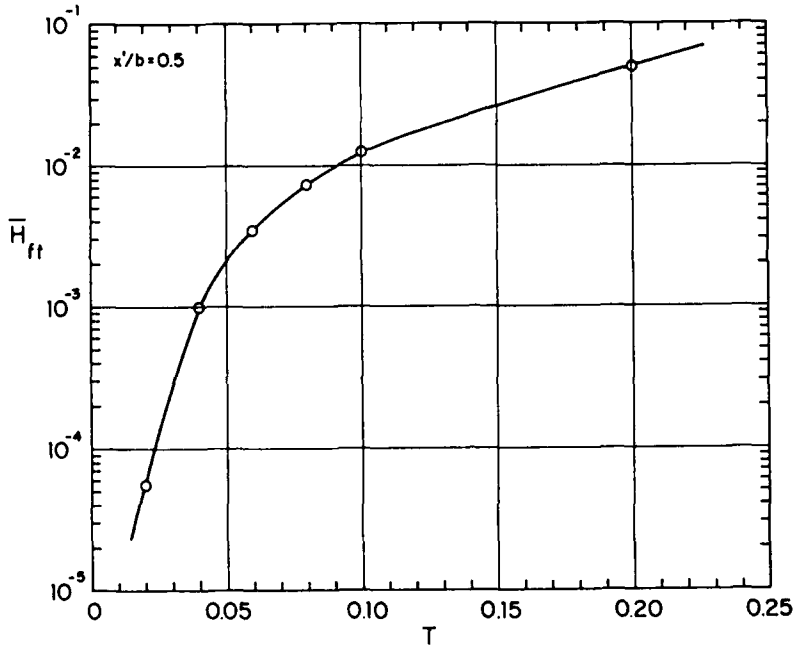

Figure A4. Temporal variation of $\overline{H}_{ft}$ in one-dimensional model (x'/b = 0.5).

middle of the lock wall ($X' = 0.5$). The cumulative heat-transfer quantity H_{ft} under this condition increases monotonically with T.

Table A1 lists temporal variations of the total heat flux H_{ft}, which were computed for several combinations of x' and BH (lock wall surface area protected from ice formation) when Q = 250 kW. To estimate the rate of heat transfer required to keep the concrete wall surface ice-free, the temperature gradients that appear in eq A7 were evaluated at $x = 0$. Figure A5 shows temporal variations of the normalized temperature gradient for three values of x'/b. As can be seen in this figure, the closer the heat source is to the wall surface, the larger the temperature gradient is at a given time. The heat flux H_f can then be calculated by

Table A1. Summary of computed total amount of heat transferred at $x = 0$, H_{ft} (W-hr/m^2).

Time (hours)	BH = *500 m^2*	BH = *250 m^2*	BH = *50 m^2*
Case 1: Q = 250 kW; b = 0.3 m; x' = 0.15 m			
1	0.6	1.2	5.8
2	11.6	23.3	116.3
3	58.1	116.3	581.4
4	116.3	232.6	1162.8
5	232.6	465.1	2325.6
Case 2: Q = 250 kW; b = 0.2 m; x' = 0.10 m			
1	9.3	18.6	93.0
2	79.1	204.7	790.7
3	158.1	317.4	1581.4
4	303.5	608.1	3034.9
5	594.2	1188.4	5941.9

$$H_f = -K\frac{\partial\theta}{\partial x} = -\frac{Q}{BH}\frac{\partial\Theta}{\partial X}. \qquad \text{(A10)}$$

Relationships between T and H_f computed for five values for Q/BH using eq A10 are shown in Figure A6. These curves were obtained for the case of a heating plate placed in the middle of the wall ($x'/b = 0.5$).

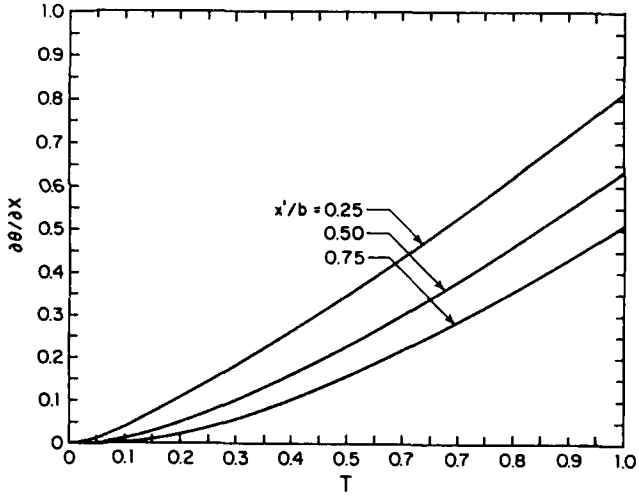

Figure A5. Temporal variations of temperature gradient for different x′/b *values.*

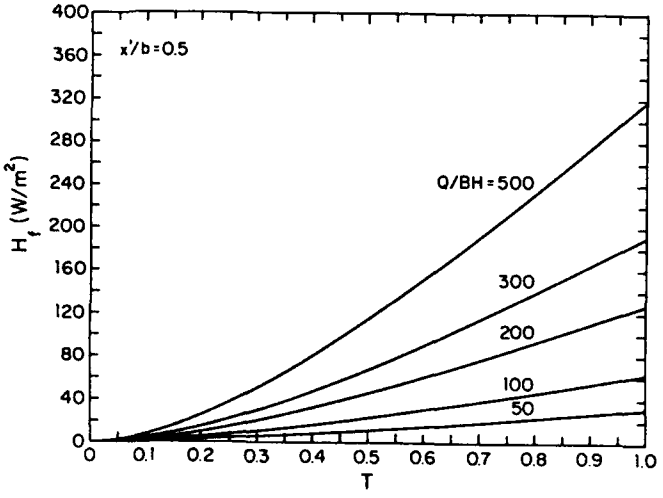

Figure A6. Temporal variation of H_f *for different* Q/BH *values* (x′/b = *0.5*).

The simple one-dimensional, plane-source model presented here was investigated to demonstrate its capability for estimating the necessary amount of heat and time of application that are required to maintain the lock wall ice-free. Needless to say, this model is crude and makes various assumptions to simplify the problem to obtain practical, simple engineering solutions.

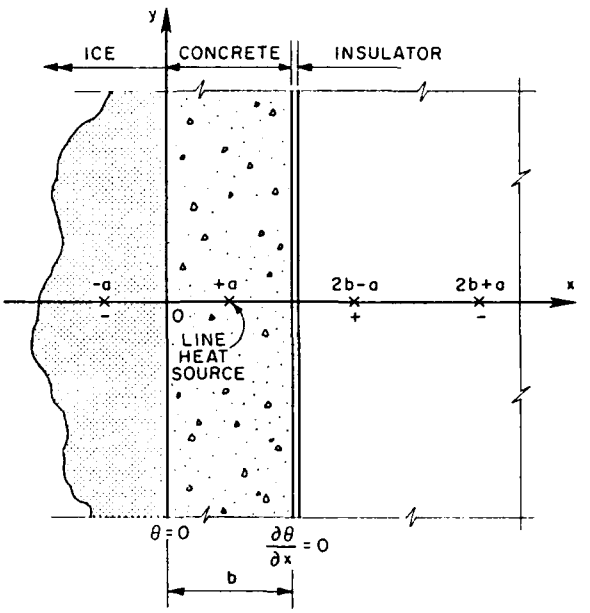

Figure A7. Definition sketch of line-heat-source model.

TWO-DIMENSIONAL HEAT-DIFFUSION MODEL

Consider a two-dimensional temperature distribution for which a steady line heat source is placed in a concrete lock wall parallel to the x-axis direction (perpendicular to the x–y plane), as shown in Figure A7. It is assumed that the line source is located at a point $(a,0)$ and that the continuous steady heat is liberated at a rate of $\rho c_p q$ per unit length and per unit time (W/m). The governing equation in this case is

$$\frac{\partial \theta}{\partial t} = k\left(\frac{\partial^2 \theta}{\partial x^2} + \frac{\partial^2 \theta}{\partial y^2}\right). \tag{A11}$$

A general solution of eq A11 is

$$\theta = \frac{q}{4\pi k}\int_{\left(\frac{r^2}{4kt}\right)}^{\infty} \frac{e^{-u}}{u}\,du = E_i\left(\frac{r^2}{4kt}\right) \tag{A12}$$

where θ = temperature (°C)
q = line-source strength (°C m^2/s)
k = heat diffusivity (m^2/s)
t = time (s)
u = dummy variable
$r^2 = (x-a)^2 + y^2$
E_i = exponential integral.

If the same boundary conditions (eq A3) as used in the previous case are imposed, it is necessary to superimpose a line sink at $(-a,0)$ to satisfy the boundary condition at $x = 0$, and a line sink and a source at $(2b+a,0)$ and $(2b-a,0)$, respectively, to satisfy the boundary condition at $x = b$. The solution to eq A12 is

$$\theta = E_i\left[\frac{(x-a)^2+y^2}{4kt}\right] - E_i\left[\frac{(x+a)^2+y^2}{4kt}\right] + E_i\left[\frac{(x-2b+a)^2+y^2}{4kt}\right] - E_i\left[\frac{(x-2b-a)^2+y^2}{4kt}\right]. \tag{A13}$$

This equation can be normalized as

$$\Theta = \frac{\theta}{\left(\frac{q}{4\pi k}\right)} = E_i\left[\frac{(X-a/b)^2+Y^2}{4T}\right] - E_i\left[\frac{(X+a/b)^2+Y^2}{4T}\right] + E_i\left[\frac{(X-2+a/b)^2+Y^2}{4T}\right]$$

$$- E_i\left[\frac{(X-2-a/b)^2+Y^2}{4T}\right] \qquad \text{(A14)}$$

where $X = x/b$
$Y = y/b$
$T = kt/b^2$.

Distributions of the normalized temperature θ at $T = 0.1$ are shown in Figure A8 for $a/b = 0.5$ (the line source is located in the middle of the lock wall) and three values of Y: 0, 0.25 and 0.50. Because of the low heat conductivity of concrete, heat transfer is extremely poor in the vertical (y) direction. For example, at $Y = 0.5$ (horizontal plane that is $0.5b$ above the axis), θ is less than one-third of its value at $X = 0.15$ in comparison with that when $Y = 0$ (Fig. A7). The value of θ for $Y = 0$ at $X = 0.5$ is approximately 31.78, and the curve in the vicinity of $X = 0.5$ is not shown in Figure A8. Figure A9 shows lateral distributions of θ at $T = 0.10$ and

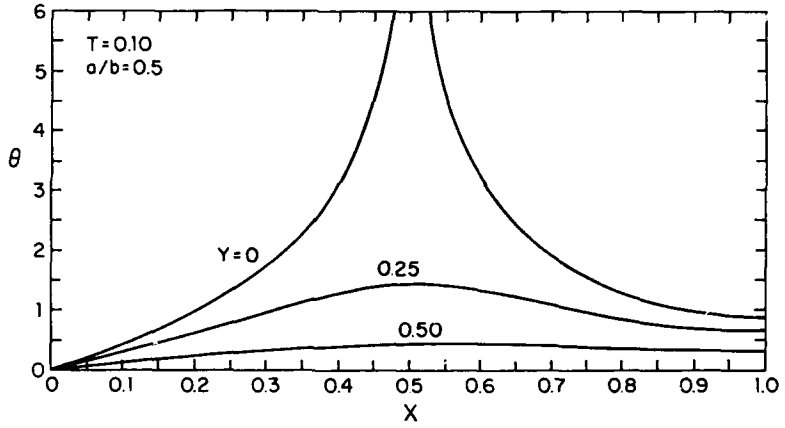

Figure A8. Spatial distributions of normalized temperature in two-dimensional model (a/b = 0.5 and T = 0.10).

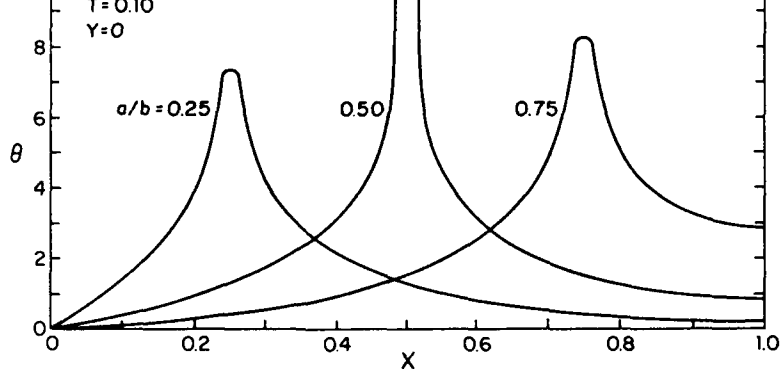

Figure A9. Spatial distributions of normalized temperature in two-dimensional model (T = 0.10 and Y = 0).

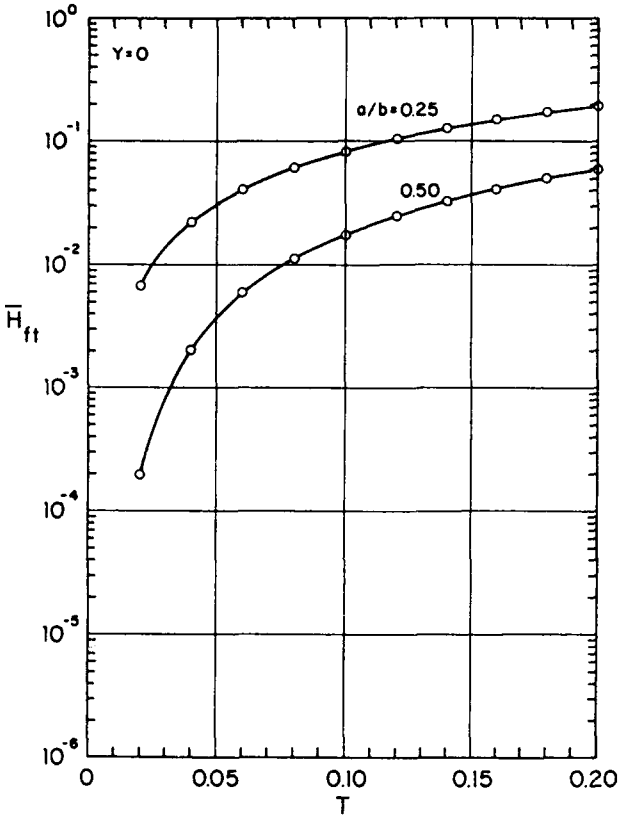

Figure A10. Temporal distributions of $\bar{H}_{ft}$ (Y = 0).

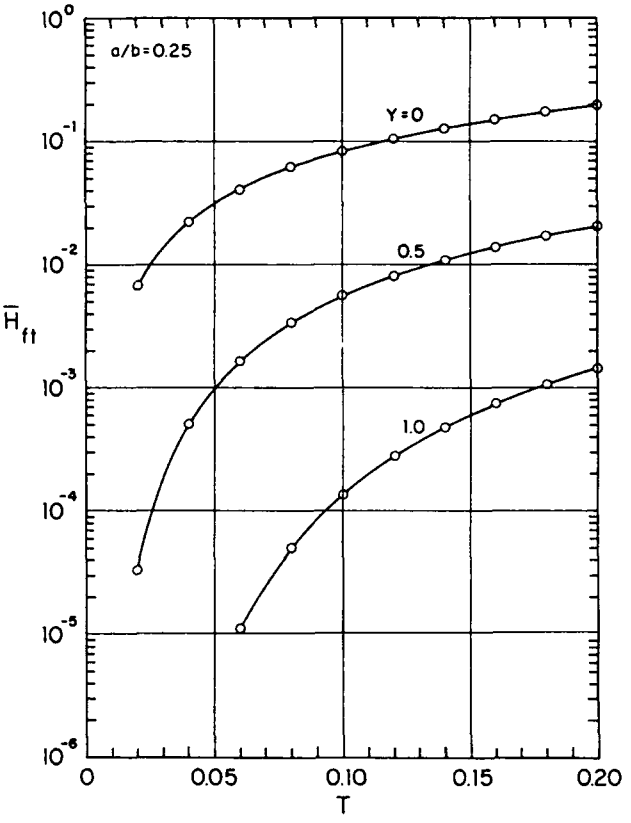

Figure A11. Temporal distributions of $\bar{H}_{ft}$ (a/b = 0.25).

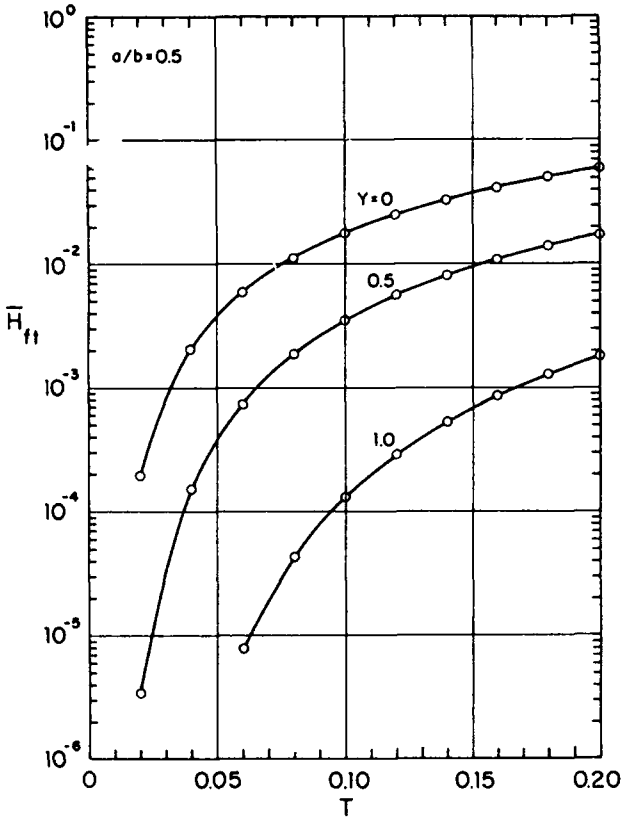

Figure A12. Temporal distributions of $\bar{H}_{ft}$ (a/b = 0.50).

$Y = 0$ for three values of a/b: = 0.25, 0.50 and 0.75. The line heat source located closer to the lock wall (see the curve for a/b = 0.25, for example) produces a larger temperature gradient at $X = 0$ than those located farther from the lock wall. This means that more heat flux is available to melt ice at a given time with a smaller value of a/b. At $T = 0.1$, values of θ near the face of the lock wall ($X = 0.1$) are 1.467, 0.444 and 0.145 for $a/b = 0.25$, 0.50 and 0.75 respectively. Heat tends to build up at X = 1 for a larger value of a/b.

To estimate the rate of heat transfer from the concrete lock wall to ice, the heat flux H_f at $X = 0$ was calculated using the following expression:

$$H_f = -K \left.\frac{\partial \theta}{\partial x}\right|_{x=0} \qquad \text{(A15)}$$

where H_f is in W/m^2 and K is the thermal conductivity in W/m·°C. The phase change of ice due to conducted heat at the lock wall boundary was not considered for simplicity's sake. The total heat flux H_{ft} accumulated in time t at $X = 0$ can be obtained by integrating H_f as

$$H_{ft} = \int_0^t H_f \, dt = \int_0^t \left(-K \frac{\partial \theta}{\partial x}\right) d \qquad \text{(A16)}$$

where H_{ft} is in W hr/m^2. Introducing eq A13 into eq A16 yields, after some mathematical manipulations, the following solution for $\bar{H}_{ft}$:

$$\bar{H}_{ft}(Y) = \frac{H_{ft}}{\rho c_p q (b^2/k)}$$

$$= -\frac{1}{2\pi}\int_0^T \left[\frac{2A}{A^2+Y^2}\exp\left(-\frac{A^2+Y^2}{4T}\right)\right.$$

$$+\frac{(2-A)}{(2-A)^2+Y^2}\exp\left[-\frac{(2-A)^2+Y^2}{4T}\right]$$

$$\left.-\frac{(2+A)}{(2+A)^2+Y^2}\exp\left[-\frac{(2+A)^2+Y^2}{4T}\right]\right] d\tau \qquad \text{(A17)}$$

where $A = a/b$. Figure A10 presents the relationships between $\bar{H}_{ft}$ and T at $Y = 0$ for $a/b = 0.25$ and 0.50, and shows the sensitivity of $\bar{H}_{ft}$ to the location of a heat source. By placing a line source at the quarter point from the lock wall ($a/b = 0.25$), the total heat flux $\bar{H}_{ft}$ accumulated in time T is seen to be approximately ten times greater than that for the case of $a/b = 0.50$. Figure A11 shows the temporal variations of $\bar{H}_{ft}$ for $a/b = 0.25$ at three vertical locations (Y = 0, 0.5 and 1.0). The total heat flux is seen to decrease drastically in the vertical direction; for example, $\bar{H}_{ft}$ at $Y = y/b = 0.5$ (along a line on the lock wall, half of the concrete wall thickness b above or below the line source) is almost ten times smaller than that at $Y = 0$ and more than hundred times smaller at $Y = 1.0$ for a range of T between 0 and 0.20. Similar trends are seen in Figure A12 when the line source is located along the center of the lock wall ($a/b = 0.5$). This analysis clearly demonstrates that the two-dimensional line heat source is not effective in maintaining ice-free conditions over a significant portion of the lock wall because the majority of the heat transfer at the lock wall boundary takes place only in the vicinity of $Y = 0$. Table A2 summarizes the results of sample computations of the total heat flux H_{ft} (W hr/m^2) with a line-source strength of $q = 11.8$°C m^2/s, which corresponds to, for example, a case in which $Q = 250$ kW is applied to a 100-m-long line source. As stated previously, there can be seen strong gradients of the heat flux in the vertical direction in this table.

Table A2. Summary of computed total amount of heat transfer H_{ft} (W hr/m^2) for a line heat-source model.

Time	*CASE 1:* a = *0.15 m*, b = *0.30 m*		*CASE 2:* a = *0.075 m*, b = *0.30 m*	
(hours)	y = *0 m*	y = *0.15 m*	y = *0 m*	y = *0.15 m*
2	442	23	6,395	105
4	3,721	500	23,256	1,047
6	9,419	1,628	45,349	2,674

Time	*CASE 3:* a = *0.10 m*, b = *0.20 m*		*CASE 4:* a = *0.05 m*, b = *0.20 m*	
(hours)	y = *0 m*	y = *0.10 m*	y = *0 m*	y = *0.10 m*
1	279	23	4,419	81
2	2,209	291	12,791	640
3	4,535	965	20,698	1,512
4	8,372	2,093	28,605	2,674
5	11,628	3,140	41,860	4,186

Note: $q = 11.8$°C m^2/s.

TWO-DIMENSIONAL HEAT-DIFFUSION MODEL IN A RECTANGULAR BOUNDARY

To heat roller-gate seals, as used for most lock and dam installations along the upper Mississippi River, it is common to provide concrete support piers with a vertical rectangular pocket in which two heating rods are inserted to inhibit ice formation on the gate seals. A typical configuration is shown in Figure A13. The rectangular pocket is assumed to be surrounded by a metal conductor at the lock wall surface and three insulated walls.

The governing equation for heat flux from the heating rods is given in eq A11; however, new boundary conditions must be imposed as follows:

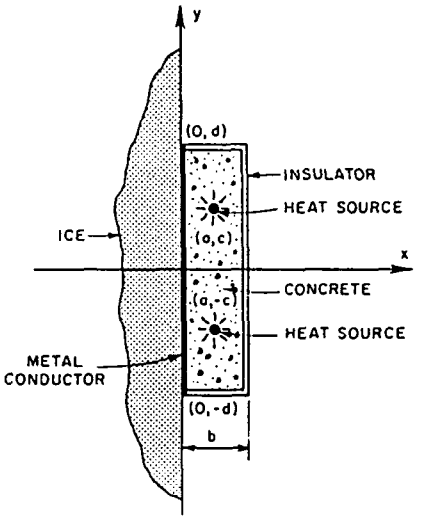

Figure A13. Definition sketch of line-heat-source model in a rectangular boundary.

$$\left.\begin{aligned} &\theta = 0°C \qquad \text{at } x = 0;\ -d \le y \le d\ (t > 0) \\ &\frac{\partial \theta}{\partial x} = 0 \qquad \text{at } x = b;\qquad -d \le y \le d\ (t < 0) \end{aligned}\right\} \tag{A18}$$

and

$$\left.\frac{\partial \theta}{\partial x} = 0 \qquad \text{at } 0 \le x \le b;\qquad y = \pm d\ (t > 0).\right\}$$

If two line heat sources are placed at (a,c) and $(a,-c)$, Sommerfeld's method of images (Carslaw and Jaeger 1947) can be applied, as shown in Figure A14, to determine the temperature distribution throughout the heated pocket. An expression for normalized heat flux H_f at $X = 0$ can be obtained in a similar manner to that used earlier. The expression is

$$\bar{H}_f(Y,T) = \frac{H_f}{\left(\frac{Q}{bH}\right)} = -\frac{1}{2\pi}\sum_{i=1}^{4}\left\{\frac{2A}{A^2+Y_i^2}\exp\left(-\frac{A^2+Y_i^2}{4T}\right)\right.$$
$$\left. + \frac{(2-A)}{(2-A)^2+Y_i^2}\exp\left[-\frac{(2-A)^2+Y_i^2}{4T}\right] - \frac{(2+A)}{(2+A)^2+Y_i^2}\exp\left[-\frac{(2+A)^2+Y_i^2}{4T}\right]\right\} \tag{A19}$$

where $Y = y/b$
$T = kt/b^2$
Q = total heat-source strength (W)
i = subscript for location of image
b = depth of the rectangular pocket (m)
H = height of ice-covered portion of lock wall (m)
H_f = heat flux at $x = 0$ (W/m^2)
$A = a/b$
$Y_1 = Y - c/b$
$Y_2 = Y - 2d/b + c/b$
$Y_3 = Y + c/b$
$Y_4 = Y + 2d/b - c/b.$

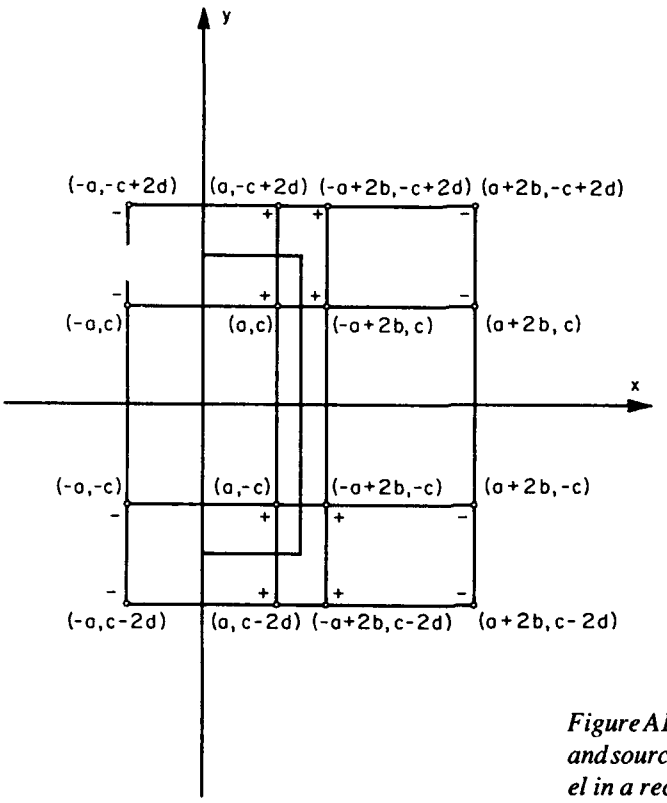

Figure A14. Locations of imaginary sinks and sources for the line-heat-source model in a rectangular boundary.

The normalized total amount of heat expended $\overline{H}_{ft}$ is determined by integrating eq A19 over T:

$$\overline{H}_{ft}(Y,T) = \frac{H_{ft}}{\left(\frac{Q}{bH}\right)\left(\frac{b^2}{k}\right)} = \int_0^T \overline{H}_f(Y,T)\, dT. \tag{A20}$$

The area-averaged normalized total amount of heat expended $\overline{H}_{fta}$ is

$$\overline{H}_{fta}(T) = \frac{H_{fta}}{\left(\frac{Q}{2dH}\right)\left(\frac{b^2}{k}\right)} = \int_{-d/b}^{d/b} \overline{H}_{ft}(Y,T)\, dY. \tag{A21}$$

$\overline{H}_{fta}$ was numerically integrated, the results of which are presented in Figures A15 and A16 as a function of T. Figure A15 shows the effect of d/b (the aspect ratio of the rectangular pocket) for fixed values of $a/b = 0.5$ (heat sources located along the centerline of the pocket) and $c/b = 2.0$. The aspect ratio is important for very small values of T; however, the effect is seen in the figure to diminish for T greater than about 0.05. Figure A16 similarly shows the effect of c/b (the positions of the rods in the y direction) for $a/b = 0.5$ and $d/b = 4.0$. These results demonstrate that $\overline{H}_{fta}$ is not significantly influenced, except for the time period close to heat application, by either the location of the rods or the length of the pocket for the given pocket depth b.

Table A3 depicts a practical example of how much heat is transferred through the metal conductor of the pocket in the lock wall under the following conditions: $Q = 5$ kW, $H = 2$ m, $a = 0.05$ m, $b = 0.10$ m, $c = 0.20$ m and $d = 0.40$ m. The total amount of heat expended H_{fta} is shown in the table as a function of time t. According to this table, approximately 1.18 kW hr/m^2 of heat can be accumulated in approximately 60 minutes. According to the lockmaster at

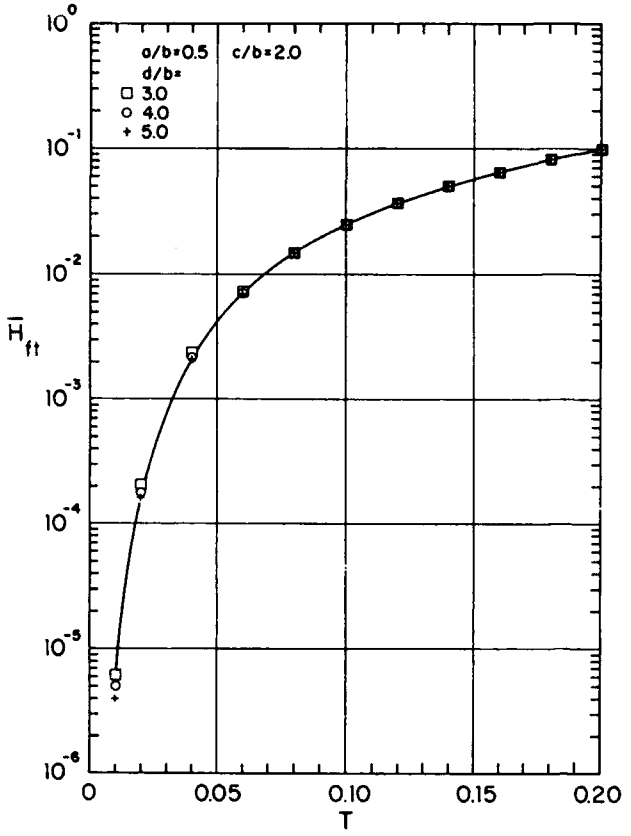

Figure A15. Temporal distributions of H_{fta} (a/b = 0.50 and c/b = 2.0)

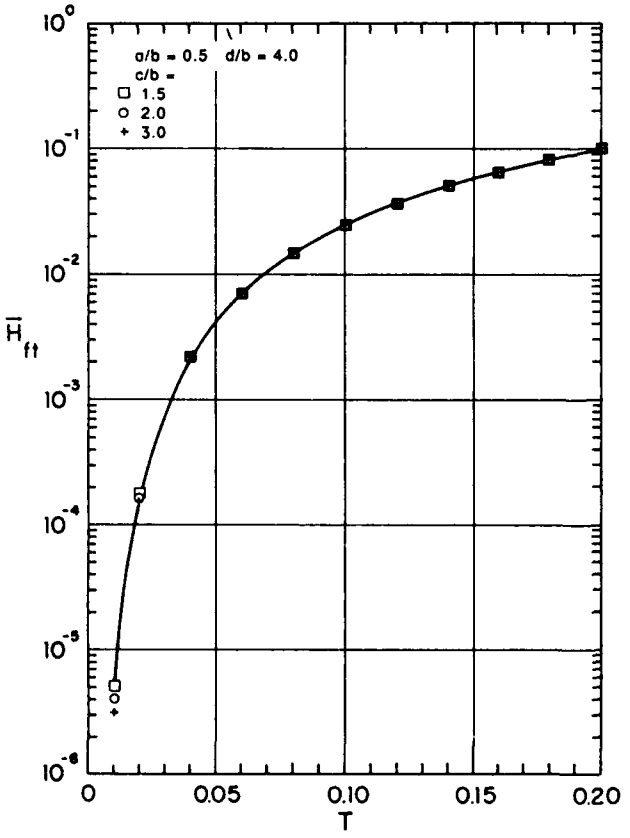

Figure A16. Temporal distributions of H_{fta} (a/b = 0.50 and d/b = 4.0).

Lock and Dam 6 located in Trempealeau, Wisconsin, along the Mississippi River, the de-icing task with side-seal heaters can be accomplished within about 45 minutes of their application. Therefore, the estimation presented above is quite encouraging, although the analytical solution was obtained under various simplifying assumptions. Also encouraging is a study that supports the present estimate, that of Balanin et al. (1986), who found that it took about 3 hours under –20°C air temperature to remove thick ice (0.15–0.20 m thick) from the wall by applying 1.5–2.0 kW hr/m^2 of electricity by means of metal strips buried in the concrete wall. According to Balanin et al. (1986), thick ice formed on the lock wall tends to slide off the wall surface due to gravity even before the temperature of the concrete wall surface reaches 0°C. The results of the present study shown in Table A3 are practically on the same order of magnitude in all variables involved. Therefore, the simple analytical solution developed in the present study could be used effectively in estimating the heating efficiency of the method of heating side seals commonly practiced by the U.S. Army Corps of Engineers.

Table A3. Summary of computed total amount of heat transfer for a two-dimensional model in rectangular boundary.

Time, t (min)	*Dimensionless time, T*	$\bar{H}_{fta}$	H_{fta} *(W-hr/m^2)*
10	0.025	0.00032	6.6
20	0.050	0.0040	82.6
30	0.075	0.012	247.7
40	0.100	0.023	474.9
50	0.125	0.039	805.2
60	0.150	0.057	1,176.7

a = 0.05 m H = 2 m
b = 0.10 m k = 4.2 × 10^{-7} m^2/s
c = 0.20 m Q = 5 kW
d = 0.40 m

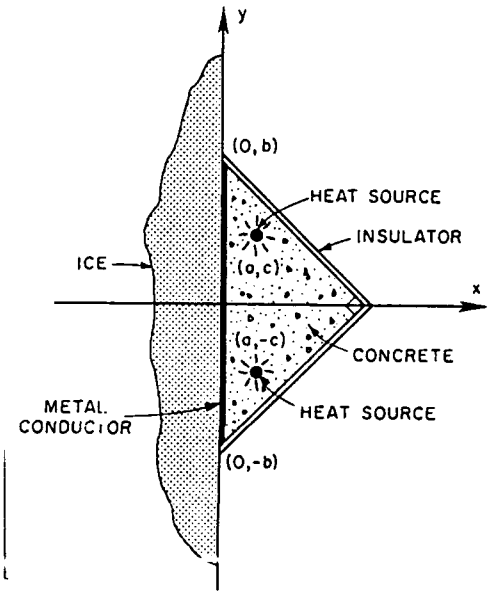

Figure A17. Definition sketch of line-heat-source model in a triangular boundary.

TWO-DIMENSIONAL HEAT-DIFFUSION MODEL IN A TRIANGULAR BOUNDARY

Consider two line heat sources that are placed in a triangular domain of a lock wall in which the hypotenuse of an isosceles right triangle is the ice–concrete boundary made of a metal conductor, as shown in Figure A17. The governing equation is given by eq A11, and the boundary conditions are

$$\left.\begin{aligned} &\theta = 0°C \quad \text{at } x = 0;\ -b \le y \le b\ (t > 0) \\ &\text{and} \\ &\frac{\partial \theta}{\partial n} = 0 \quad \text{along insulated boundary} \end{aligned}\right\} \tag{A22}$$

where n is normal to the sides of the triangle. To satisfy these boundary conditions, imaginary sources and sinks are necessary, as shown in Figure A18. The normalized heat flux $\bar{H}_f$ is

$$\bar{H}_f(Y,T) = \frac{H_f}{\left(\frac{Q}{bH}\right)} = -\frac{1}{2\pi}\left\{\sum_{i=1}^{6} \frac{\ell_i}{\ell_i^2 + (Y - m_i)^2} \exp\left[-\frac{\ell_i^2 + (Y-m_i)^2}{4T}\right]\right\} \tag{A23}$$

where $Y = y/b$

$T = kt/b^2$

i = subscript for location of the image

b = half of the wall width

h = height of the wall

$\ell_1 = \ell_2 = a/b$

$\ell_3 = \ell_4 = 1 - c/b$

$\ell_5 = \ell_6 = 1 + c/b$

$m_1 = -m_2 = c/b$

$m_3 = -m_4 = 1 - a/b$

$m_5 = -m_6 = a/b - 1.$

Therefore, the normalized total amount of heat $\bar{H}_{ft}$ expended over normalized time T is

$$\bar{H}_{ft}(Y,T) = \frac{H_{ft}}{\left(\frac{Q}{bH}\right)\left(\frac{b^2}{k}\right)} = \int_0^T \bar{H}_f(Y,T)\,dT. \quad \text{(A24)}$$

The area-averaged normalized total amount of heat $\bar{H}_{fta}$ is

$$\bar{H}_{fta}(T) = \frac{H_{fta}}{\left(\frac{Q}{2bH}\right)\left(\frac{b^2}{k}\right)} = \int_{-1}^{1} \bar{H}_{ft}(Y,T)\,dY. \quad \text{(A25)}$$

$\bar{H}_{fta}$ was computed as a function of T for three cases, and the results are shown in Figure A19. Case 3 in Figure A19 represents the case in which a single rod is placed at $(a,0)$ where $a = 0.5b$. The single heat source is less efficient than those cases with two heating rods, in particular, for small T. Table A4 lists the results of the computed total heat

Table A4. Summary of computed total amount of heat transfer for a two-dimensional model in triangular boundary.

T	t (min)	$\bar{H}_{fta}$	H_{fta} (W hr/m²)
Case 1: a/b = 0.25, c/b = 0.25			
0.010	15.9	9.8E-5	16.2
0.015	27.8	4.3E-4	71.0
0.020	31.7	1.0E-3	165.2
0.025	39.7	1.9E-3	313.8
0.030	47.6	3.0E-3	495.6
0.035	55.6	4.2D-3	693.8
0.040	63.5	5.7E-3	941.6
0.050	79.4	9.0E-3	1486.7
Case 2: a/b = 0.30, c/b = 0.30			
0.010	15.9	1.8E-5	3.0
0.015	23.8	1.2E-4	19.8
0.020	31.7	3.6E-4	59.4
0.025	39.7	7.6E-4	125.6
0.030	47.6	1.3E-3	214.8
0.035	55.6	2.0E-3	330.3
0.040	63.5	2.9E-3	479.1
0.050	79.4	5.0E-3	825.9
Case 3: a/b = 0.50, c/b = 0			
0.010	15.9	3.5E-6	0.6
0.015	23.8	3.9E-5	6.4
0.020	31.7	1.5E-4	24.8
0.025	39.7	3.8E-4	62.8
0.030	47.6	7.5E-4	123.8
0.035	55.6	1.2E-3	198.3
0.040	63.5	1.9E-3	313.8
0.050	79.4	3.5E-3	578.1

b = 0.20 m
H = 2 m
Q = 5 kW
$k = 4.2 \times 10^{-7}$ m²/s.

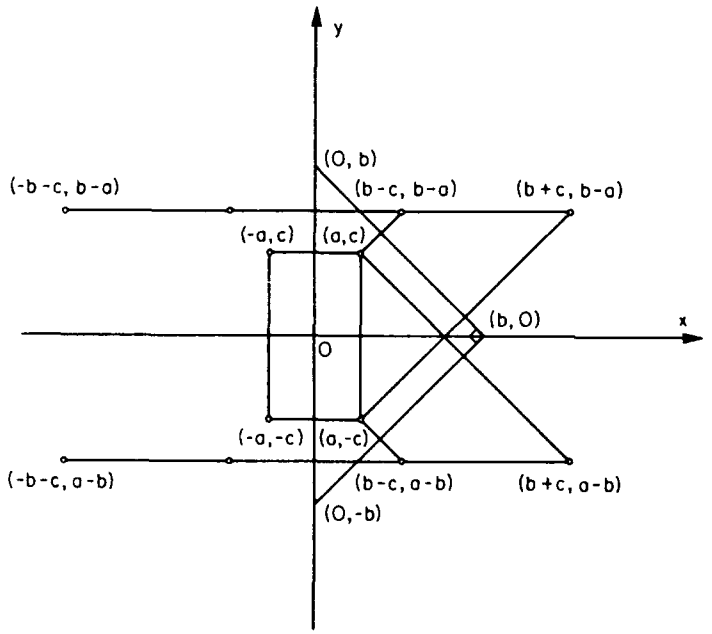

Figure A18. Locations of imaginary sinks and sources for the line-heat-source model in a triangular boundary.

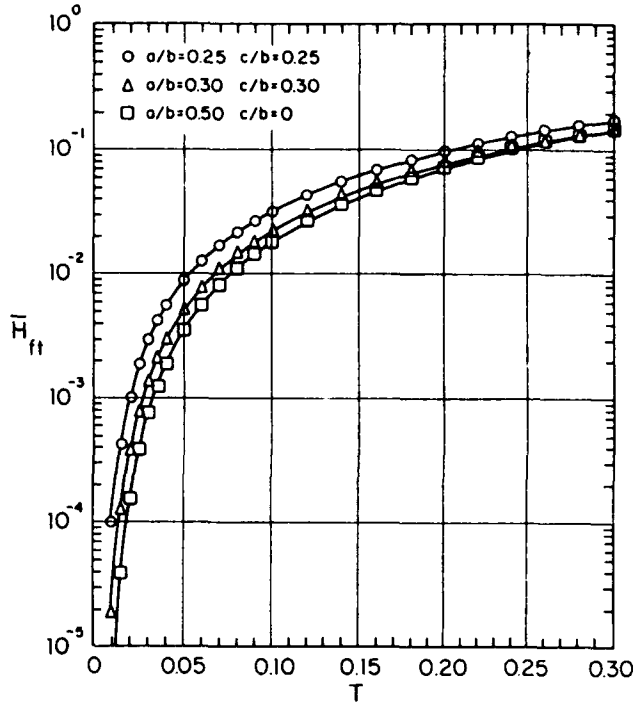

Figure A19. Temporal distributions of H_{fta} for different a/b *and* c/b *values.*

transferred in time for each of the three cases presented in Figure A19. It was assumed that $b = 0.20$ m, $h = 2$ m and $Q = 5$ kW (or 2.5 kW per each heating rod). For example, the total amounts of heat transferred at the wall boundary after applying heat for 40 minutes ($T = 0.025$) are about 314, 126 and 63 W hr/m^2 for cases 1, 2 and 3, respectively.

APPENDIX B: MATHEMATICAL FORMULATION OF INCOMPLETE MIXING OF GROUNDWATER IN A LOCK CHAMBER

The system of heat fluxes depicted in Figure B1 may be expressed as

$$\phi_{wa} = \rho_w Q C_p \left(T_g - T_{sw}\right) + \frac{k_w}{h_t}\left(T_{wL} - T_f\right) LW \tag{B1}$$

in which the second term on the right side refers to heat conducted through the body of lock water, T_{sw} is the surface temperature of water ($T_{sw} > T_f$) and T_{wL} is the water temperature in the lower layer of the lock chamber. As an approximation, one might assume $T_{wL} = 4°C$. Using

$$\phi_{wa} = H_{wa}(T_{sw} - T_a)\, LW \tag{B2}$$

eq B1 becomes

$$Q = \frac{H_{wa} LW(T_{sw} - T_a)}{\rho_w C_p (T_g - T_{sw})} - \frac{k_w LW(T_{wL} - T_f)}{h_t \rho_w C_p (T_g - T_{sw})}$$

$$= \frac{LW}{\rho_w C_p}\left[H_{wa}\frac{(T_{sw} - T_a)}{(T_g - T_{sw})} - \frac{k_w}{h_t}\frac{(T_{wL} - T_f)}{(T_g - T_{sw})}\right]. \tag{B3}$$

It is assumed in the foregoing that groundwater discharge cools from T_g to T_{sw}, the surface water temperature, before descending to the lower part of a lock chamber.

In eq B3 the thickness and temperature of the lower layer are not constant. Layer thickness h_t increases with time:

$$h_t = \frac{1}{LW}\int_0^t Q\,dt \tag{B4}$$

with boundary conditions: $h_t = 0$ at t = 0; and $h_t = D$ when $t = LWD/Q$. Layer temperature decreases at a rate

$$\frac{dT_w}{dt} = \frac{1}{h_t}\left[\frac{k_w}{\rho_w C_p}\left(T_{wL} - T_{wf}\right)\right] = \frac{Q}{LW}\left(T_g - T_{sw}\right). \tag{B5}$$

Equations B3, B4 and B5 must be solved jointly and numerically.

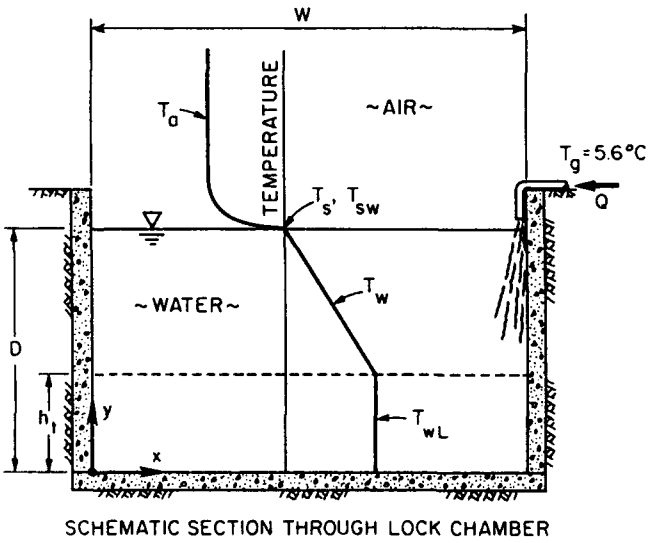

SCHEMATIC SECTION THROUGH LOCK CHAMBER

Figure B1. Temperatures associated with incomplete mixing of groundwater in a lock chamber.

REPORT DOCUMENTATION PAGE

Form Approved
OMB No. 0704-0188

1. AGENCY USE ONLY (Leave blank)	2. REPORT DATE	3. REPORT TYPE AND DATES COVERED
	June 1992	

4. TITLE AND SUBTITLE

Unconventional Energy Sources for Ice Control at Lock and Dam Installations

5. FUNDING NUMBERS

Contract No. DACW89-86-K-001

6. AUTHORS

Tatsuaki Nakato, Robert Ettema and Keiichi Toda

7. PERFORMING ORGANIZATION NAME(S) AND ADDRESS(ES)

Iowa Institute of Hydraulic Research
The University of Iowa
Iowa City, Iowa

8. PERFORMING ORGANIZATION REPORT NUMBER

9. SPONSORING/MONITORING AGENCY NAME(S) AND ADDRESS(ES)

U.S. Army Cold Regions Research and Engineering Laboratory
72 Lyme Road
Hanover, New Hampshire 03755-1290

and

Office of the Chief Engineers
River Ice Management Program
Washington, DC 20314-1000

10. SPONSORING/MONITORING AGENCY REPORT NUMBER

Special Report 92-13

11. SUPPLEMENTARY NOTES

12a. DISTRIBUTION/AVAILABILITY STATEMENT

Approved for public release; distribution is unlimited.

Available from NTIS, Springfield, Virginia 22161.

12b. DISTRIBUTION CODE

13. ABSTRACT (*Maximum 200 words*)

Operation of lock and dam installations is made troublesome and hazardous by ice growth along lock walls and by freezing of gates to ice covers. Since considerable amounts of power are required for ice control, lock operators are interested in utilizing economical power sources other than that generated by commercial utilities. This study attempted to determine the feasibilities of using several unconventional power sources for ice control at navigation locks and dams. Considered were sensible heat from groundwater, solar power, wind power and portable hydroelectric sources. Only portable hydroelectric power is feasible. Groundwater is at best of marginal feasiblity, and solar and wind power sources are unreliable.

14. SUBJECT TERMS

Dams Ice control Locks

15. NUMBER OF PAGES
41

16. PRICE CODE

17. SECURITY CLASSIFICATION OF REPORT	18. SECURITY CLASSIFICATION OF THIS PAGE	19. SECURITY CLASSIFICATION OF ABSTRACT	20. LIMITATION OF ABSTRACT
UNCLASSIFIED	UNCLASSIFIED	UNCLASSIFIED	UL

NSN 7540-01-280-5500

Standard Form 298 (Rev. 2-89)
Prescribed by ANSI Std. Z39-18
298-102

☆ U.S. GOVERNMENT PRINTING OFFICE: 1992-600-063/60007